LITERATURE REVIEW ON FATIGUE BEHAVIOR OF REINFORCED CONCRETE BRIDGE DECKS

Project Task Report

By

Xun Wang and Lijuan "Dawn" Cheng

Department of Civil and Environmental Engineering, University of California, Davis

Prepared for the

California Department of Transportation (Caltrans)

March 2023

ABSTRACT

The current AASHTO LRFD Bridge Design Specification does not require investigating the fatigue needs for reinforced concrete (RC) deck slabs in multi-girder applications or reinforced concrete box culverts. However, design truck loads for bridge and truck volume have been continuously increasing since the 1960's. The truck loads and wheel configurations that the bridge decks are designed per AASHTO specification no longer reflect the modern trucks, not mentioning the use of larger permit vehicles (e.g., P-15 in CA) and legal vehicles such like special hauling vehicles (SHV) and emergency vehicles (EV) in the design. Hence, it is a worthy practice to conduct a comprehensive literature review survey on the state-of-art fatigue models of RC deck slab and estimate its fatigue life subjected to the current truck axle load for design considerations.

Two major levels of fatigue models are investigated and reviewed in this report, including fatigue models for plain concrete at the material level, and fatigue models for RC bridge deck slab at the structural level. For plain concrete, the fatigue behavior subjected to cyclic loading is introduced in terms of residual concrete strength, secant modulus, and concrete strain. Important factors on the fatigue performance of plain concrete are discussed, such as normalized stress level and stress ratio, stress reversal, multi-axial stress state, loading frequency, shape of cyclic loading form, and loading history. Fatigue models from available literatures on plain concrete are reviewed and categorized by different theoretical basis, which include deterministic models, probabilistic models, and energy models. In aspect of the fatigue models for RC bridge deck slab, experimental studies under both static and fatigue load cases are firstly introduced to illustrate the failure mechanism of RC deck slab subjected to tire patch load. Different approaches are then described to estimate the static load capacity of RC deck slab, including various punching shear models and yield line theory. Available semi-empirical fatigue life models in the literatures are summarized to provide the most practical references for the fatigue design of RC deck slabs. Additionally, studies on using numerical method to explore the fatigue failure process of RC deck slab are also introduced, even though the modeling strategy to account for the fatigue degradation is complicated. Finally, two potential

frameworks are recommended by the authors to adopt the current fatigue models into practical design, namely, the stress-based method and the force-based method. And a case study within the scope of the force-based method is presented as an example to calculate the fatigue life of typical RC bridge deck slabs in CA with the provided design inputs.

TABLE OF CONTENT

LIST OF FIGURES

LIST OF TABLES

1 INTRODUCTION

Fatigue is a slow process of mechanical degradation of a material when it is confronted with repeated loading (Torrenti et al. 2013). It is an irreversible process of deterioration in the microstructure of the material, in a form of diffuse microvoids or microcracks, and results in a permanent damage of the material. The material can fail under a load level much smaller than its static load-carrying capacity when the number of applied cycles is sufficient. However, repeated loadings with a very high load level, e.g., earthquakes may cause failures in less in than 100 cycles [ACI 215R-74 (Revised 1992/Reapproved 1997)]. These failures are usually referred to as low-cycle fatigue and will not be specifically discussed in this report.

Many cementitious or reinforced concrete (RC) elements of infrastructures are subjected to repeated loadings, such as airport and highway pavement, highway and railway bridges and bridge decks. They will mostly experience a high-cycle fatigue with an approximate range from 1000 to 10 million cycles during their service life (Hsu 1981). Among these RC elements as described above, RC bridge decks were prone to have fatigue failure after decades of service. Although the fatigue failures of other RC elements are rarely observed in the existing structures, the degradation in structural performance under fatigue loading may lead to many serious problems. For example, the development of internal microcracks of concrete elements under fatigue loading can accumulate to macro-cracks, resulting in a loss of stiffness and strength of the concrete elements. The infiltrated moisture and chloride salt through the concrete cracks may cause the reinforcement to corrode and further weaken the performance of the entire structure (Sun et al. 2002). On the other hand, with the increase of live load because of the heavier modern trucks, existing bridges are expected to carry a larger ratio of live load to dead loads. The repeated load amplitude applied to the bridge components (deck, girder and columns, etc.) will become larger and accelerates the deterioration of materials, which may lead to a shortened service life. Thus, it is important to understand the fatigue behavior at both the material level and the structural level for RC elements. The fatigue effects should also be recognized in the design to ensure that the in-service load ranges of the structural component remain at an appropriate level to accommodate the design life.

This research aims at conducting a comprehensive literature review on the fatigue behavior of RC bridge deck, as well as the available models for design considerations. Because the failure process of RC bridge decks subjected to cyclic loads is usually governed by the degradation of concrete material, the factors that affect the fatigue performance of plain concrete are the main focuses of this discussion. Fatigue models of plain concrete are also collected and categorized from the open literature, which contains different model types based on the average concrete strength, probability of failure and dissipated energy. To fully understand the failure mechanism of RC bridge deck under fatigue loading, experimental studies are focused to expose the typical structural behavior of RC deck slabs under static, fixed pulsating and moving wheel loading cases. The degraded behavior of RC deck slabs and cracking patterns of concrete is discussed in detail based on the test observations. In addition, different theories are reviewed to explore the failure process of RC deck slabs subjected to tire patch loads, along with the semi-empirical models derived from the test data to predict the fatigue life of RC deck slabs. Numerical methods are also presented as a potential alternative to the time- and cost-consuming experimental studies, despite the complicated modeling of materials to consider the degradation under fatigue loading.

2 FATIGUE OF PLAIN CONCRETE

2.1 Overview

Plain concrete element subject to cyclic loads may fail after a number of cycles, which is referred to as the fatigue life *N*, although the maximum stress that the concrete element has experienced is less than the concrete strength (compressive or tensile). The fatigue life *N* of concrete is usually interpreted by a logarithmic relation with the maximum applied normalized stress level S_{max}, with the minimum applied normalized stress level S_{min} remains constant. Herein, S_{max} and S_{min} equals to the maximum and minimum stress level during the repeated loading with respect to the static strength of concrete (compressive or tensile), respectively. If S_{max} is in tension, a positive S_{min} represents a tension-tension cyclic loading, and a negative S_{min} represents a tension-compression cyclic loading and vice versa. This relation is usually referred to as the Wöhler curve, also known as the *S*-*N* curve.

For example, as shown in Fig. 2-1, the series of *S*-*N* curves represent the fatigue life expectations under different S_{min} in tension. It can be seen that, with the increase of S_{min}, the fatigue life N increases under the same S_{max}. This type of *S*-*N* curves predicted by the deterministic models, reflecting the experimental observations, are most common and has been widely adopted by many researchers (Tepfers and KuttiHsu 1979; Hsu 1981; Cornelissen and Reinhardt 1984; Petkovic et al. 1990; Lohaus et al. 2012; Isojeh et al. 2017). It neglects the variations in the static concrete strength and use either the characteristic or the average concrete strength to determine the normalized stress levels (S_{max} and S_{min}).

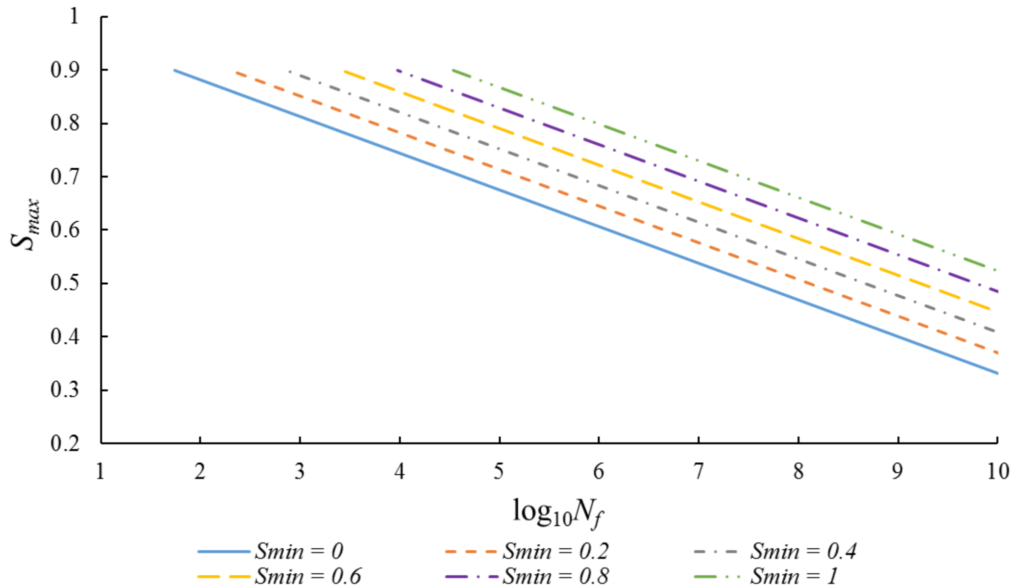

Fig. 2-1 Predicted S-N curves for plain concrete in tension (adapted from Cornelissen and Reinhardt 1984)

However, to obtain reliable *S*-*N* curves for design, a large number of concrete specimens needs to be tested for each stress level, yet significant scatter in *S*-*N* data is still inevitable due to the variation of concrete strength within the same batch, as well as the stochastic nature of fatigue process (Cornelissen and Reinhardt 1984). This scatter exists in both the static and fatigue strength of concrete and depends on the same parameters, including but not limited to nature and type of the aggregates, concrete mix proportions, water to cement ratio, porosity, curing condition, size of the specimen, loading rate, concrete shrinkage and creep, etc.

To address the aforementioned scattering issue and to estimate the fatigue life of concrete specimen, the probabilistic concept has been incorporated into the fatigue model by many researchers (McCall 1958; Holmen 1982; Petryna et al. 2002; Saucedo et al. 2013; Liang et al. 2017; Ortega et al. 2018). For example, as shown in Fig. 2-2, a series of *S*-*N* curves are presented for different probability of failure (*P*) of concrete, and these are usually called as the *S*-*N*-*P* curves. In general, the curve of 50% probability of failure (P = 0.5) is adopted to describe the behavior of concrete under fatigue loading.

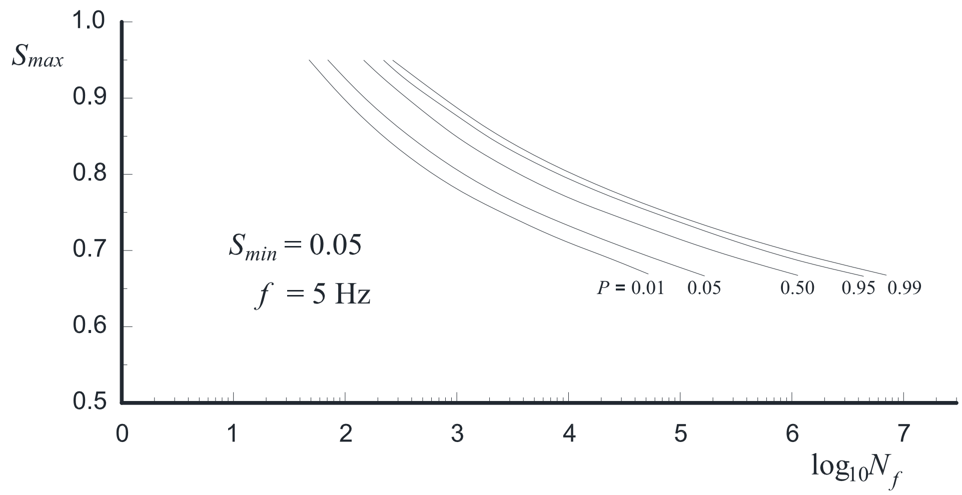

Fig. 2-2 Representative *S-N-P* curves based on a linear interpolation for the probability of failure (adapted from Holmen 1982)

2.2 Fatigue behavior of concrete

The development of fatigue in concrete is basically a degenerative process of the material. The energy absorbed by the concrete within each fatigue cycles leads to the diffuse microcracks and it causes the internal damage to accumulate. For concrete material, this energy is referred to as the dissipation energy E_δ within each cycle enclosed by the unloading and reloading path, as shown in Fig. 2-3. The area between the first loading and the first unloading curve represents the irreversible plastic energy E_{pl} of the concrete. The area under the first unloading curve represents the elastic energy E_{el}. The reloading curve is above the first unloading curve, but with a smaller stiffness than the initial one. The major part of the dissipation energy E_δ is believed to be transformed into thermal energy and the cumulative dissipated energy ΣE_δ is related to the damage process of the concrete (Bode and Marx 2020).

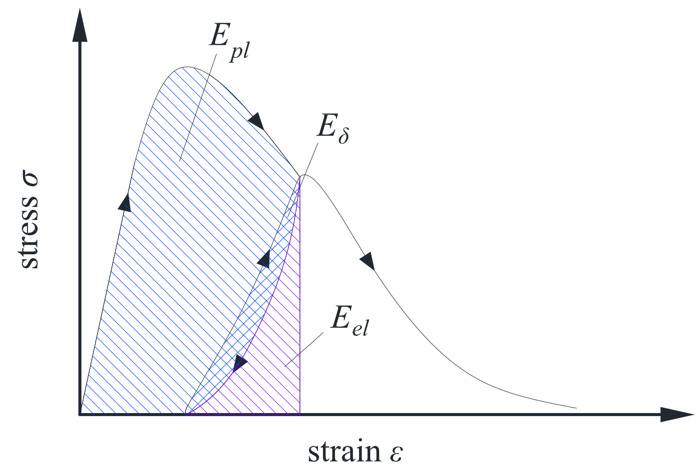

Fig. 2-3 Stress-strain behavior of concrete under cyclic loading (adapted from Bode and Marx 2020)

On the other hand, with the development of internal damage of concrete under cyclic loading, the mechanical properties of concrete will vary gradually, including residual concrete strength, secant modulus, and concrete strain.

2.2.1 Residual concrete strength

Research aims to investigate the residual concrete strength after a specific number of fatigue cycles is rare. Isojeh et al. (2017) tested a series of concrete cylinders and measured their residual compressive strength before the fatigue failure. It was found that the residual compressive strength of concrete slightly increased at early fatigue cycles, but with a further increase of cycles, an obvious degradation in compressive strength was observed. A similar observation was also noticed in the test of Taliercio and Gobbi (1996) where the residual strength of the specimens survived the target fatigue cycles under uniaxial load reached a larger strength than their static counterparts on average. But those specimens with extra lateral confinement presented a lower post-fatigue compressive strength than their static counterparts. The early increase of the post-fatigue compressive strength maybe due to the further curing of concrete and scatter of concrete material. However, it is generally believed that the fatigue cycles will have a detrimental effect on the residual concrete strength because of the accumulated internal damage (Petryna et al. 2002).

2.2.2 Secant modulus

For concrete specimens tested under fatigue cycles and reached fatigue failure, a common three-stage behavior was observed for the secant modulus of concrete. In Fig. 2-4, the secant modulus of concrete started to decrease rapidly not long after the fatigue cycles started, and this stage is referred to as the first stage. The decrease rate of the secant modulus then slowed down and reached a relative stable magnitude, this second stage usually accounted for over 70% of the fatigue life N_f of the concrete specimen. When the concrete specimen was close to its fatigue life, the decrease rate of the secant modulus speeded up again until fatigue failure. This three-stage behavior was noticed not only in the compressive concrete fatigue test (Holmen 1982; Petkovic et al. 1990; Gao and Hsu 1998), but also in the flexural and torsional fatigue tests of plain concrete as well (Subramaniam et al. 2000; Subramaniam et al. 2002). In addition, the decrease rate of secant modulus is highly relevant to the maximum stress level applied to the specimen, as presented in Fig. 2-4. Taliercio and Gobbi (1996) also found out that for specimens under triaxial fatigue load conditions, the greater internal damage caused by a higher stress triaxiality ratio resulted in a more significant drop in the secant modulus.

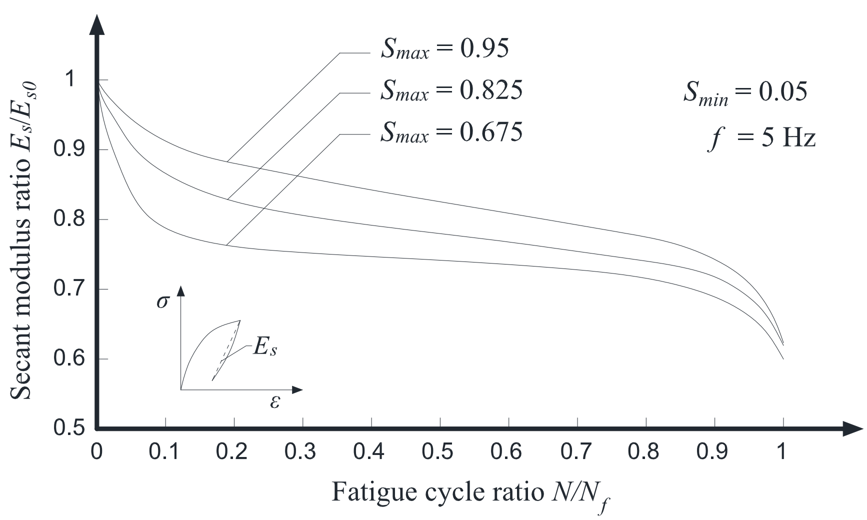

Fig. 2-4 Representative change in secant modulus of plain concrete during fatigue cycles (adapted from Holmen 1982)

2.2.3 Concrete strain

Likewise, the permanent strain of concrete performed in a three-stage development during the fatigue cycles, as shown in Fig. 2-5, but its magnitude always increased as compared to the decreasing trend of secant modulus as presented in Fig. 2-4. At the first stage (typically within 10-20%N_f), the concrete strain had a nonlinear increase at a decreasing rate due to the closing up of concrete pores and microcracks between aggregates and cement mortar. It was followed by a stable increase with a constant rate in the second stage, while the microcracks within the cement mortar increased. Researchers reported that the duration of the second stage usually stayed within 70-90%N_f (Holmen 1982; Cornelissen and Reinhardt 1984; Taliercio and Gobbi 1996; Isojeh et al. 2017), beyond which the strain increased rapidly again in the third stage until fatigue failure.

Because of the relative stable strain rate within the second stage, some researchers believed it is more reliable to predict the fatigue life of plain concrete by using the "secondary strain rate ε_{sec} (or secondary creep rate)", as illustrated in Fig. 2-5. As a result, a general equation was proposed by Sparks and Menzies (1973) to estimate the fatigue life N_f as below:

$$N_f = a(\varepsilon_{sec})^{-b} \tag{2.1}$$

where a, b= coefficients calibrated from the test data.

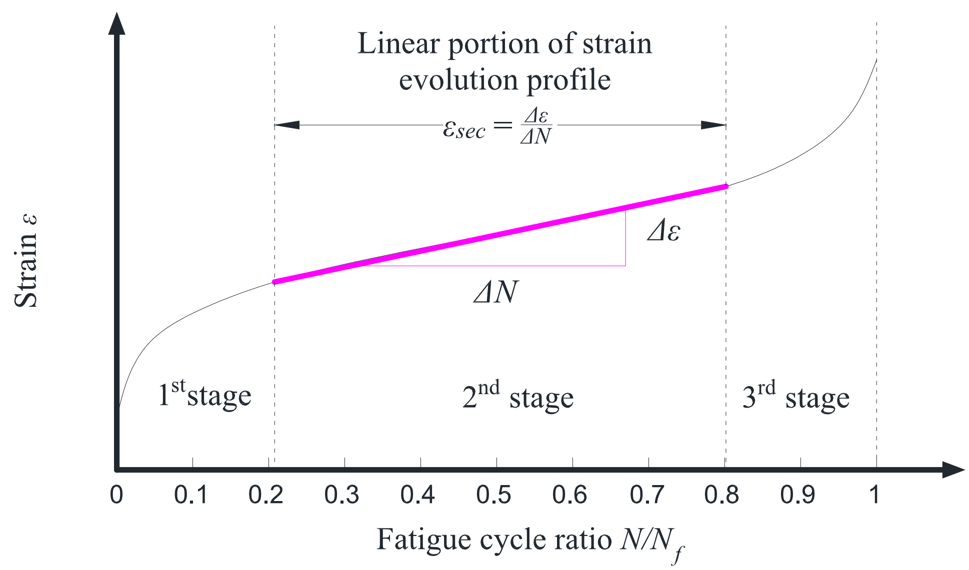

Fig. 2-5 Concrete strain development during the fatigue cycles (adapted from Isojeh et al. 2017)

2.3 Important parameters of concrete fatigue

Due to the lack of standard test configuration for the plain concrete under fatigue loading, the reported fatigue tests of concrete in the literatures used different test setups, size and geometry of the concrete specimens. To minimize the influence caused by these testing details, the normalized fatigue parameters are usually preferred in the fatigue models to accommodate the test data from different experiments. In short, the fatigue life of concrete primarily depends on the key parameters as below, which will be discussed in the subsections:

- Normalized stress level and stress ratio (or amplitude)
- Stress reversal
- Multi-axial stress state
- Loading frequency
- Shape of cyclic loading form
- Loading history

2.3.1 Normalized stress level and stress ratio

From test observations in the open literatures, the normalized stress level, both the maximum normalized stress level S_{max}, and the minimum normalized stress level S_{min} play the most important role in the fatigue life of concrete. Test results from Cornelissen and Reinhardt (1984) indicated that for tested concrete specimens under repeated loading, at a given S_{max}, reducing S_{min} resulted in shorter lives of concrete specimens. In other words, a larger stress amplitude, i.e., (S_{max} - S_{min}), means a shorter fatigue life. On the other hand, Aas-Jakobsen (1970) reported that the relationship between S_{max} and S_{min} is linear for concrete specimens failed at 2 million fatigue cycles. And hence, he proposed the famous Aas-Jakobsen's formula to incorporate the stress ratio R, which equals to S_{min}/S_{max}, into the Wöhler curve and yielded the following fatigue model as:

$$S_{max} = 1 - \beta(1 - R)log_{10}N_f \tag{2.2}$$

where β = material parameter (0.0685 per Aas- Jakobsen 1970). This model has been widely adopted by researchers to examine the fatigue life of concrete and a typical illustration of this model is shown in Fig. 2-6. This model was also further extended by other studies to take more factors into consideration (Hsu 1981; Zhang et al. 1996; Isojeh et al. 2017).

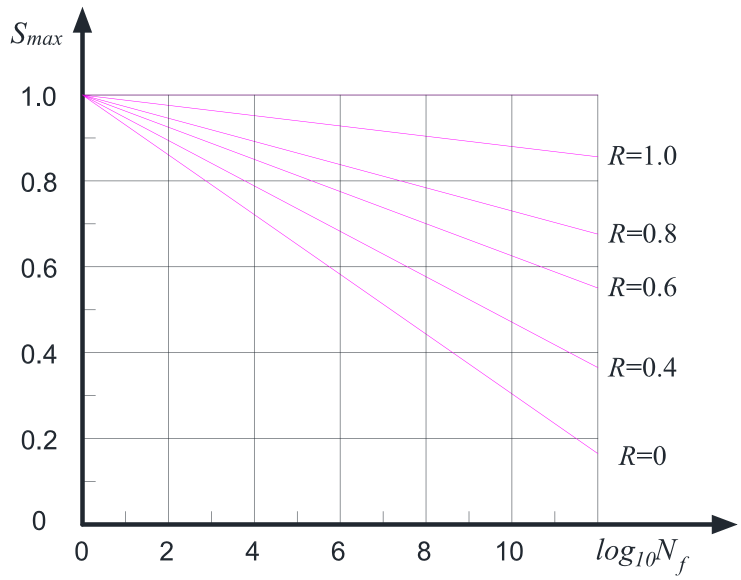

Fig. 2-6 Wöhler curves for different values of *R* (adapted from Tepfers and Kutti 1979)

However, it should be noted that for a very large R number, e.g., R = 1, Eq. (2.2) yields a result of S_{max} = 1. It basically means that the concrete is under the sustained loading condition instead of the fatigue loading. Tests conducted by Rüsch (1960) indicated that the sustained strength of concrete is time dependent, and the long-term strength may drop down to 75-80% of the short-term static strength due to concrete creep. Therefore, it is generally believed that for R > 0.75, the concrete specimen is approaching the sustained loading state and this sustained loading effect should be considered for fatigue models (Tepfers et al. 1973; Hsu 1981; Zhang et al. 1996; Zhang et al. 1998).

2.3.2 Stress reversal

Few experimental studies were reported on the stress reversal effect on the fatigue performance of plain concrete. Cornelissen and Reinhardt (1984) tested a series of plain concrete specimens under both tensile and tensile-compressive fatigue loading. Test results indicated that at a given maximum tensile stress level, when the minimum stress was reversed from tensile to compressive, a considerable reduction of fatigue life was observed. This detrimental effect of stress reversal from tension-tension to tension-compression was also confirmed by Reinhardt and Cornelissen (1984). A modified Goodman diagram is presented herein to visualize the effect due to the stress reversal (Cornelissen and Reinhardt 1984). In Fig. 2-7, each curve represents the relationship between the maximum and minimum stress level when the specimen can reach a fatigue life of the designated number, e.g., $\log N_f = 3$. The vertical axis indicates the normalized maximum tensile stress level, while the horizontal axis indicates the normalized minimum stress level either in tension or compression. It should be noted that for the tension-tension condition the normalized minimum stress level is based on the tensile strength of concrete, while it is based on the compressive strength of concrete for the tension-compression condition. Apparently in this plot, the stress reversal will lead to a shorter fatigue life of specimens. To reach the same fatigue life, e.g., $\log N_f = 5$, it is necessary to remain a much lower maximum tensile stress for the tension-compression condition. Although the negative effect caused by the stress reversal on the fatigue life of plain concrete was also confirmed by both Tepfers (1982) and Zhang et al. (1996), they believed that the influence of stress reversal is small.

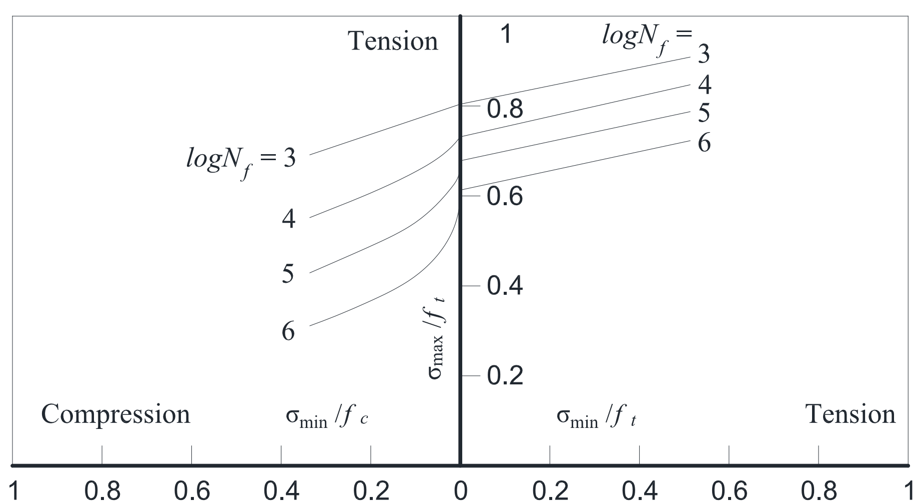

Fig. 2-7 Modified Goodman diagram of concrete under stress reversal (adapted from Cornelissen and Reinhardt 1984)

2.3.3 Multi-axial stress state

Limited studies were conducted aiming to investigate the influence of multi-axial stress state on the fatigue behaviors of plain concrete. Although the experimental study conducted by Buyukozturk and

Tseng (1984) did not focus on the fatigue life of concrete under biaxial stress state, test results indicated that the lateral confinement contributed to the stiffness of the specimen in the inelastic range during cyclic loading. Su and Hsu (1988) reported that the biaxial compression state detained the internal microcracks of concrete, and hence it prolonged the fatigue life compared to the uniaxial compression state. As shown in Fig. 2-8, a series of biaxial fatigue strength envelops are plotted covering the fatigue life from one cycle to 10 million cycles with a constant stress ratio $R = 0.05$. Each envelop represents the relationship between the two orthogonally applied normalized stress level, i.e., $\sigma_2/f_c^{'}$ and $\sigma_3/f_c^{'}$, at the designated fatigue life of the concrete specimen. It was concluded that a maximum increase of fatigue strength could be achieved at the confining stress ratio σ_2/σ_3 equals to either 0.2 or 0.5 for a target fatigue life of two million cycles. On the other hand, Taliercio and Gobbi (1996) tested a series of concrete specimens under triaxial compressive stress state. Again, test results confirmed that the lateral confinement increased the fatigue life of concrete specimen, but it also caused more internal damage of concrete material and led to a more rapid decrease in the residual modulus.

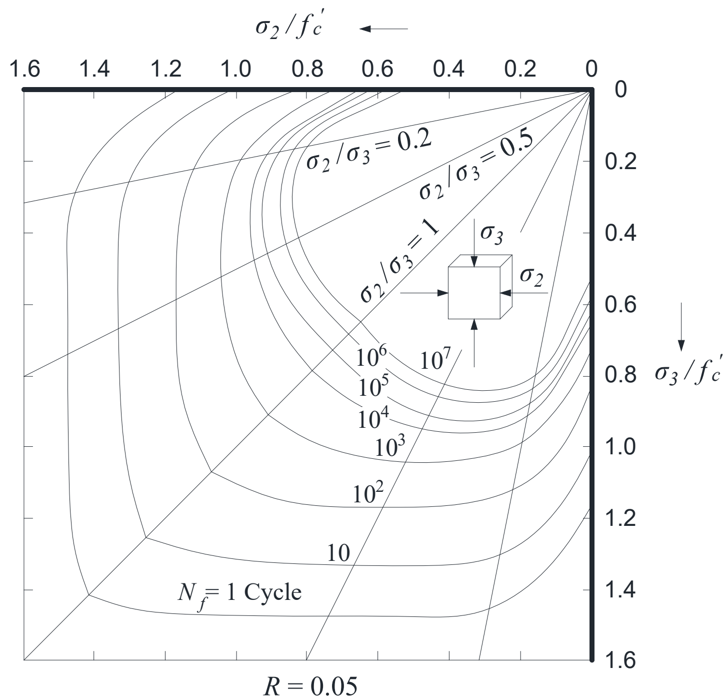

Fig. 2-8 Fatigue strength envelope of concrete under biaxial compressive stress state (adapted from Su and Hsu 1988)

2.3.4 Loading frequency

The loading frequency, or the rate of loading during fatigue cycles, is believed to have little effect on the fatigue strength of concrete within the range of approximately 1-15 Hz, provided that the normalized maximum stress level S_{max} is less than 75% [ACI 215R-74 (Revised 1992/Reapproved 1997)]. But for concrete specimens with $S_{max} > 0.75$, the effect due to the loading frequency becomes more significant because of the concrete creep (Sparks and Menzies 1973; Tepfers and Kutti 1979, Zhang et al. 1996). Under a higher stress level, decreasing the rate of loading equals to changing the concrete stress state from the fatigue loading to the sustained loading, hence the long-term effect is non-negligible as described above in section 2.3.1. In addition, the tests conducted by Ode and Marx (2020) also indicated that more damage was accumulated within each fatigue cycle for concrete specimens under a lower frequency in the aspect of energy dissipation. Furthermore, Zhang et al. (1996) proposed an equation to measure the actual concrete strength f_{cf}' at the applied loading frequency f, and the equation is presented as follows:

$$f_{cf}' = C_f f_c' = \left(ab^{-logf} + c\right) f_c' \tag{2.3}$$

where a, b = material parameters = 0.249, 0.920, respectively; and c = coefficient of long-term concrete strength = 0.796. This equation indicates that the long-term concrete strength is approximately 80% of the static strength when the loading frequency approaches zero. Likewise, Hsu (1981) incorporated the time effect and the effect of loading rate into the Aas-Jakobsen's formula to estimate the fatigue life of concrete, and this model will be introduced in detail later in this review study.

2.3.5 Shape of cyclic loading form

As aforementioned in section 2.3.4, the sustained loading effect will influence the fatigue life of plain concrete because of the creep. In this sense, Zhang et al. (1998) tested a few concrete beam specimens to investigate the relation between the sustained load level and the sustained time to failure. The proposed model was similar to the model firstly introduced by Hsu (1981); however, it also took the shape of cyclic loading forms (square, triangular, trapezoidal and sinusoidal) into consideration by virtue of an equivalent damage assumption (Zhang et al. 1998). A transformation coefficient ω was hence introduced to convert the cyclic period t_0 into an equivalent time t_{max} under the maximum applied fatigue load level S_{max}. In Fig. 2-9, the shape of the cyclic loading form depends on the shape factor λ, which varies within the range between 0 and 1. Fig. 2-10 provides the values of ω corresponding to different shape factors λ and special stress ratios R', where R' can be represented by the following equations to account for the effect due to stress reversals as well:

$$\begin{aligned} R' &= R = \frac{S_{min}}{S_{max}} \quad for\ R \geq 0 \\ R' &= \left|\frac{f_r}{f_c'}\right| R \qquad for\ R < 0 \end{aligned} \tag{2.4}$$

where f_r = modulus of rupture of concrete; and f_c' = concrete compressive strength.

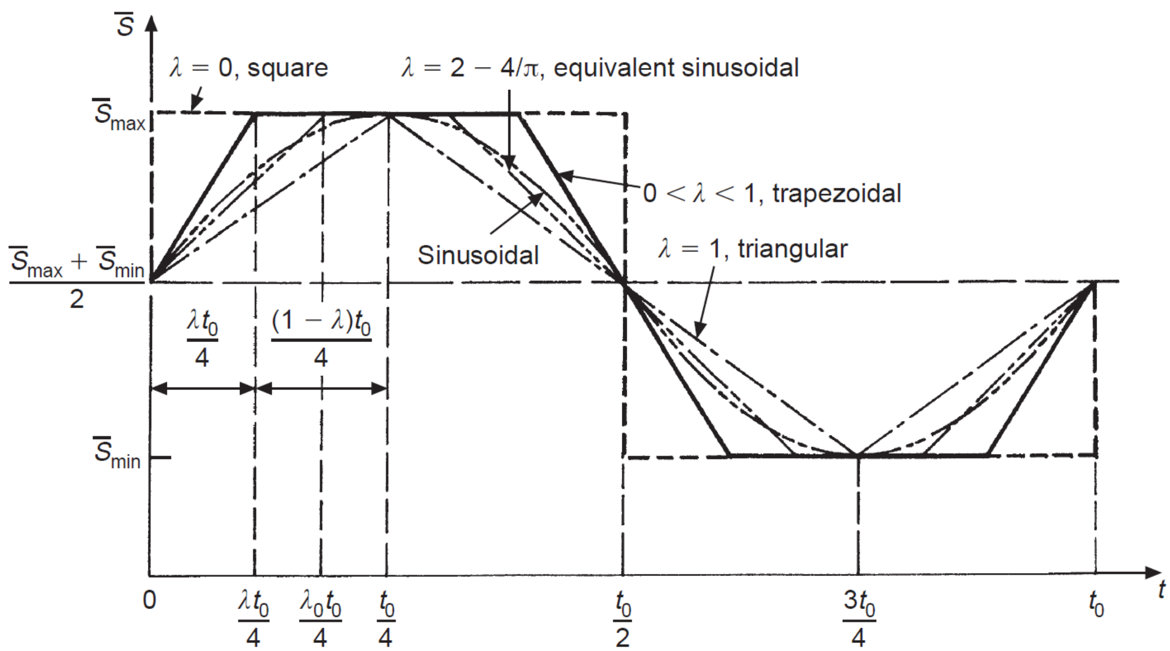

Fig. 2-9 Full trapezoidal loading cycles for different λ (Zhang et al. 1998)

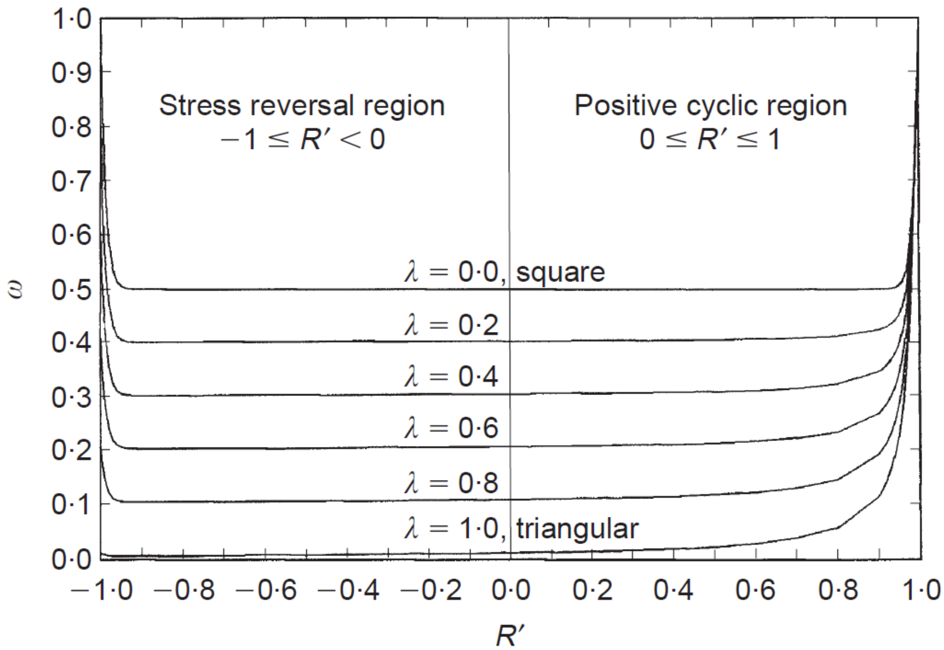

Fig. 2-10 Family of ω - R' curves for different λ (Zhang et al. 1998)

2.3.6 Loading history

Most experimental studies reported in the literatures adopted constant fatigue stress amplitudes (range) to test the concrete specimens up to failure. However, this laboratory fatigue loading condition is ideal and against the nature of randomly varying loads applied to the concrete structures in the real world. To approximate more representative fatigue loading conditions, a few tests were carried out to investigate the influence of variable stress amplitudes on the fatigue life of concrete specimens (Hilsdorf and Kesler 1966; Holmen 1982; Cornelissen and Reinhardt 1984; Petkovic et al. 1990). Meanwhile, the Palmgren-Miner (PM) rule (Palmgren 1924; Miner 1945) was often taken as the failure criterion for specimens under a combination of different fatigue stress levels: The PM rule assumes that the damage D of concrete accumulates linearly with the increase of fatigue cycles under constant maximum and minimum stress levels, and it reaches unity when the fatigue failure occurs. In the case of varying stress amplitude conditions, the equivalent damage can be calculated by:

$$D = \sum_{i=1}^{k} \frac{N_i}{N_{fi}} = 1.0 \tag{2.5}$$

where i = i^{th} stress amplitude condition; k = total number of different stress amplitude conditions; N_i = number of fatigue cycles under the i^{th} stress amplitude condition; N_{fi} = number of fatigue cycles to failure under the i^{th} stress amplitude condition. It assumes that the damage caused by each stress amplitude condition can be added linearly to the equivalent damage and it neglects the sequential effect of different stress amplitude conditions. Although this PM rule was widely adopted in many studies, the fatigue life of concrete specimen predicted by the PM rule can be either unsafe (e.g., $D < 1$) or too conservative (e.g., D > 1) at specimen failure in different test programs (Hilsdorf and Kesler 1966; Holmen 1982; Cornelissen and Reinhardt 1984). As a result, the concept of non-linear accumulation of damage extended from the PM law was also proposed by some researchers (Torrenti et al. 2013) to account for the sequence of various fatigue stress amplitudes.

2.4 Fatigue life models of concrete

The scatter of fatigue life of concrete specimens is significant and unpredictable according to the existing experimental data. For identical concrete specimens in the same batch, the scatter in concrete fatigue life can reach as much as two orders of magnitude or even higher (Ortega et al. 2018). To minimize the variations caused by this scatter of material properties, fatigue models of concrete are usually proposed and calibrated from a large number of test specimens. As aforementioned in the overview, the deterministic model has been mostly adopted to predict the fatigue life of concrete, based on the average concrete fatigue strength. On the other hand, probabilistic models also draw the attention of researchers to take the dispersion of concrete properties into consideration by means of the probability of failure (Holmen 1982; Petryna et al. 2002; Saucedo et al. 2013; Liang et al. 2017; Ortega et al. 2018). Moreover, other alternative approaches have also been investigated, such as the energy-based method (Tepfers et al. 1984; Lei et al. 2017; Song et al. 2018; Bode and Marx 2021) or concrete strain-based method (Sparks and Menzies 1973; Isojeh et al. 2017). Limited by the scope of this project, not all the available fatigue models of concrete in the literatures will be discussed in this review, only those representative models are introduced in the following subsections as key references.

2.4.1 Deterministic model

Most deterministic models widely adopted are based on the Aas-Jakobsen's formula (1970) and use the stress ratio R as the most important variable, as described in section 2.3.1. Extensions or revisions of this formula are proposed by either recalibrating the model coefficients from a larger database or incorporating more parameters (Hsu 1981; Isojeh et al. 2017). Nevertheless, other forms of deterministic models were also proposed by considering the influence due to S_{max} and S_{min} on the fatigue life of concrete, respectively (Cornelissen and Reinhardt 1984; Model of Petkovic et al. 1990; Lohaus et al. 2012). Representative deterministic models of concrete fatigue life are introduced as below:

(1) *Model of Hsu (1981)*

Hsu (1981) extended the Aas-Jakobsen's formula (1970) to include the effect due to the rate of loading, or equivalently the time effect. He also investigated the differences for both low-cycle and high-cycle fatigue loading cases, as well as the boundary between these two cases. The proposed fatigue models are presented in the following:

(a) For low-cycle fatigue ($N = 1 - 10^3$):

$$S_{max} = 1.2 - 0.2R - 0.133(1 - 0.779R)logN_f - 0.053(1 - 0.445R)logt \qquad (2.6)$$

(b) For high-cycle fatigue ($N = 10^3 - 10^7$):

$$S_{max} = 1 - 0.0662(1 - 0.556R)logN_f - 0.294logt \qquad (2.7)$$

where t = period of one load cycle (sec).

(2) *Model of Isojeh et al. (2017)*

Isojeh et al. 2017 proposed a damage evolution model by combining the models of Hsu (1981), Gao and Hsu (1998) and Zhang et al. (1998) to take parameters including loading frequency, shape of cyclic loading form, stress ratio into consideration. It can also estimate the concrete residual strength and fatigue secant modulus by means of the damage concept assuming the critical damage value $D_{cr} = 0.4$ for the secant modulus, and $D_{cr} = 0.35$ for the residual strength. This damage evolution model can be presented as follows:

$$D = D_{cr}exp[s(S_{max} - u)]N^v \qquad (2.8)$$

$$u = C_f\left(1 - \gamma_2 log\left(\zeta N_f t\right)\right) \tag{2.9}$$

$$v = 0.434C_f\left(\beta_2(1 - R)\right) \tag{2.10}$$

where s = damage parameter (only valid for $0 \leq R \leq 0.5$, more details per Isojeh et al. 2017); t = period of one load cycle (sec); $\gamma_2 = 2.47\times10^{-2}$; ζ = transformation coefficient converting the cyclic period t into an equivalent time $T = 0.15$ for sinusoidal cycle (Zhang et al. 1998); C_f is referred to Eq. (2.3). It should be noted that the fatigue failure occurs when $D = D_{cr}$.

(3) *FIB Model Code 2010 (FIB 2010)*

The FIB model code 2010 prescribes the fatigue strength of concrete by the category of pure compression, compression tension and pure tension, respectively. This model is valid for concrete material with a normal strength, or high strength or even ultra-high strength (up to C200). The effects due to the age of concrete, temperature, type of concrete and sustained loading have also been considered.

(a) Pure compression (Lohaus et al. 2012):

For $S_{c,min} > 0.8$, the S-N relations for $S_{c,min} = 0.8$ are valid. For $0 \leq S_{c,min} \leq 0.8$, we can use:

$$logN_1 = \frac{8}{(Y-1)}\left(S_{c,max} - 1\right) \tag{2.11}$$

$$logN_2 = 8 + \frac{8ln(10)}{(Y-1)}\left(Y - S_{c,min}\right)log\left(\frac{S_{c,max}-S_{c,min}}{Y-S_{c,min}}\right) \tag{2.12}$$

with:

$$Y = \frac{0.45+1.8S_{c,min}}{1+1.8S_{c,min}-0.3S_{c,min}^2} \tag{2.13}$$

where:

$$\text{if } \log N \leq 8\text{, then } \log N = \log N_1 \tag{2.14a}$$

$$\text{if } \log N > 8\text{, then } \log N = \log N_2 \tag{2.14b}$$

with:

$$S_{c,max} = \frac{\left|\sigma_{c,max}\right|}{f_{ck,fat}}$$

$$S_{c,min} = \frac{\left|\sigma_{c,min}\right|}{f_{ck,fat}}$$

$$\Delta S_c = |S_{c,max}| - |S_{c,min}|$$

where $S_{c,max}$ = maximum compressive stress level (MPa); $S_{c,min}$ = minimum compressive stress level (MPa); $\sigma_{c,max}$ = maximum compressive stress (MPa); $\sigma_{c,min}$ = minimum compressive stress (MPa); and $f_{ck,fat}$ = fatigue reference compressive strength and may be estimated as:

$$f_{ck,fat} = \beta_{cc}(t)\beta_{c,sus}(t,t_0)f_{ck}(1 - f_{ck}/400) \tag{2.15}$$

In which $\beta_{cc}(t)$ = age coefficient of concrete at the beginning of fatigue loading as:

$$\beta_{cc}(t) = esp\left\{s\left[1 - \left(\frac{28}{t_T}\right)^{0.5}\right]\right\} \tag{2.16}$$

where s = coefficient which depends on the strength class of cement in Table 2-1; t_T = temperature-adjusted concrete age in days and could be determined by:

$$t_T = \sum_{i=1}^{n} \Delta t_i exp\left[13.65 - \frac{4000}{273+T(\Delta t_i)}\right] \tag{2.17}$$

where Δt_i = number of days where at a temperature T prevails; $T(\Delta t_i)$ = mean temperature in °C during the time period Δt_i.

Table 2-1 Coefficient *s* for different types of cement

f_{cm} (MPa)[a]	Strength class of cement	s
≤ 60	32.5 N	0.38
	32.5 R, 42.5 N	0.25
	42.5 R, 52.5 N, 52.5 R	0.20
> 60	All classes	0.20

[a]f_{cm} = mean compressive strength in MPa at an age of 28 days.

In addition, $\beta_{c,sus}(t,t_0)$ = coefficient which takes into account the effect of high mean stresses during loading and may be taken as 0.85 for fatigue loading; and f_{ck} = characteristic compressive strength refers to 5% quantile of static strength (Table 2-2).

Table 2-2 Characteristic strength f_{ck} of normal weigh concrete (MPa)

Concrete grade	C12	C16	C20	C25	C30	C35	C40	C45	C50
f_{ck}	12	16	20	25	30	35	40	45	50
$f_{ck,cube}$	15	20	25	30	37	45	50	55	60
Concrete grade	C55	C60	C70	C80	C90	C100	C110	C120	-
f_{ck}	55	60	70	80	90	100	110	120	-
$f_{ck,cube}$[a]	67	75	85	95	105	115	130	140	-

[a]Characteristic value of cube compressive strength of concrete.

(b) Compression-tension with $\sigma_{ct,max} \leq 0.026|\sigma_{c,max}|$:

$$logN = 9(1 - S_{c,max}) \tag{2.18}$$

(c) Pure tension and tension-compression with $\sigma_{ct,max} > 0.026|\sigma_{c,max}|$:

$$logN = 12(1 - S_{ct,max}) \tag{2.19}$$

with:

$$S_{ct,max} = \sigma_{ct,max}/f_{ctk,min}$$

where $S_{ct,max}$ = maximum tensile stress level; $\sigma_{ct,max}$ = maximum tensile stress (MPa); and $f_{ctk,min}$ = minimum characteristic tensile strength (MPa).

2.4.2 Probabilistic model

Because of the scatter in the concrete static strength and the stochastic nature of fatigue procedure, larger deviations are usually observed between the model predictions and test results by using the deterministic approaches. In the recent years, probabilistic approach of concrete fatigue failure has been developed and become a promising alternative to the deterministic model by some researchers (Petryna et al. 2002; Model of Saucedo et al. 2013; Liang et al. 2017; Ortega et al. 2018). Some representative studies are summarized as below:

(1) *Model of Ortega et al. (2018)*

Ortega et al. (2018) conducted a series of fatigue tests on the self-compacting steel fiber-reinforced concrete specimens, and a two-parameter Weibull distribution was selected to describe the cumulative probability of concrete failure under compressive cyclic load as:

$$F(x) = 1 - exp\{-(x/\eta)^{\beta}\} \tag{2.20}$$

where $x = logN$; η = scale factor (3.72 calibrated from the test data) and β = shape factor (4.56 calibrated from the test data). The scale factor η also approximately represents the order of magnitude (10^{η}) of the fatigue lifetime of concrete specimens. This research also proposed a methodology to establish the minimum number of tests needed to limit the possible error below an admissible value, and it helped determine the design fatigue curve for a given safety level.

(2) *Model of Saucedo et al. (2013)*

Saucedo et al. (2013) proposed a probabilistic fatigue model, based on a three-parameter Weibull cumulative distribution function, to describe the probability of failure (PF) and quantify the dispersion of concrete static strength as follows:

$$PF(\sigma_{f0}) = 1 - \exp\left[-\left(\frac{\sigma_{f_0} - \sigma_{min_0}}{\lambda}\right)^k\right] \qquad \sigma_{f_0} \geq \sigma_{min_0} \tag{2.21}$$

where σ_{f0} = intercept of the iso-probability failure curve with the σ_f axis; σ_{min0} = minimum stress below which no failure will occur; λ = scale parameter; and k = shape parameter. For the fatigue life N of concrete specimens, the influence of loading frequency f was also considered, along with the maximum stress σ_{max} and stress ratio R as follows:

$$PF(N; \sigma_{max}, f, R) = 1 - \exp\left\{-\left[\frac{\sigma_{max}\left(\frac{\dot{\sigma_0}}{2f\Delta\sigma}\right)^{\alpha} - \sigma_{min_0}}{\lambda N^{-[b+c\ln(1+f)](1-R)}}\right]^k\right\} \tag{2.22}$$

$\dot{\sigma_0}$ = loading rate of the compressive characterization test; $\Delta\sigma$ = stress range; α = 0.014; b and c = coefficients relevant to the loading frequency calibrated from the test data. This model can also be reformed to obtain the fatigue life in terms of the secondary strain rate $\dot{\varepsilon}$ as:

$$PF(\dot{\varepsilon}; \sigma_{max}, f, R) = 1 - \exp\left\{-\left[\frac{\sigma_{max}\left(\frac{\dot{\sigma_0}}{2f\Delta\sigma}\right)^{\alpha} - \sigma_{min_0}}{\lambda N(\dot{\varepsilon})}\right]^k\right\} \tag{2.23}$$

2.4.3 Energy model

Lei et al. 2017 proposed an energy-based fatigue model and it assumed that the dissipated energy within each cycle is based on the stress level of concrete as:

$$W_d = \alpha exp(\beta S) \tag{2.24}$$

where α = transient response coefficient of cyclic hysteretic energy (1.899×10^{-11} calibrated from the test data); β = transient response exponent of cyclic hysteretic energy of the test (28.489 calibrated from the test data); and S = stress level of concrete (MPa). This study also believed that the critical energy dissipation W_{dc}, or the accumulated energy dissipation at concrete failure, is a mechanical property of the concrete and independent of the stress level S. It can be estimated as a constant 737kJ/m^3 from the tests conducted by

Tepfers et al (1984). Hence, assuming a constant energy dissipation rate during the fatigue cycles, the fatigue life can be calculated by

$$N_f = W_{dc}/W_d \tag{2.25}$$

However, test results from Bode and Marx (2020) indicated that the accumulative energy dissipation of specimen at failure is proportional to the number of fatigue cycles, and a huge difference existed in the accumulative energy dissipation for specimens under different stress level. This conclusion contradicted with the assumptions adopted by Lei et al. (2017)

3 FATIGUE OF RC BRIDGE DECKS

3.1 Overview

The fatigue degradation of RC bridge decks is a complex hybrid process composed of concrete crack and deterioration, degradation of the bond between concrete and steel reinforcements, redistribution of internal stress, and degradation of steel reinforcements, etc. Although AASHTO (2017) does not require the fatigue design of RC deck slabs supported on multi-girders, the fatigue failure of the RC deck slabs is possible and has been confirmed in previous experiments. In addition, the fatigue life of RC deck slabs can be significantly decreased when subjected to moving wheel load, compared to the fixed pulsating load (Sonoda and Horikawa 1982; Perdikaris and Beim 1988).

On the other hand, the most common fatigue failure pattern of RC deck slabs is the punching shear failure, with significant concrete cracks developed at the bottom of the slab, along with the elliptical cracks on the top of the slab closer to the supports (Sonoda and Horikawa 1982). The only exception was reported by Schläfli and Brühwiler (1998) where the fatigue failure due to the fracture of steel rebars was observed for specimens under a high peak fatigue load. However, the tested specimens are slab-like beams with an aspect ratio equals to eight, not representative of the bridge deck slabs. And the load was applied primarily through a four-point bending setup (with no tire footprint), with the beam simply supported at the far ends. This test will not be included in this review because it significantly deviates from the typical test setup of RC bridge deck slabs subjected to patch loads. As a result, the fracture failure of reinforcements, as well the fatigue behavior of reinforcements on the material level (i.e., steel and FRP) will not be discussed herein. Nevertheless, the allowable constant-amplitude fatigue thresholds for different reinforcements are specified in Article 5.5.3 of AASHTO (2017) for other structural components of bridges.

3.2 Experimental study

Due to cost and restrictions of laboratory conditions, limited number of experimental efforts have been made to investigate the fatigue behavior of RC bridge decks under the vehicle load. Although some relevant projects have been conducted by either the department of transportations (DOTs) in different countries or the research teams at universities, full-scale field fatigue tests on the RC bridge decks are rare. Nevertheless, it is still important to understand the fatigue behavior of RC bridge decks from the reduced-scale specimens under pulsating load. Hence, some of the most representative experimental studies are reviewed and summarized in this section to disclose the fatigue characteristics of RC bridge decks under fatigue loading.

3.2.1 Deck specimens

The dimension of the concrete bridge deck specimens varies significantly for different testing purposes and highly depends on the scale factor of the experiment. For consistency, the dimensions of tested specimens have been converted to their original design dimensions according to the reported scale factor, e.g., 1/3 for the tests of Sonoda and Horikawa (1982), and Youn and Chang (1998), 1/6.6 for the test of Perdikaris and Beim (1988). The equivalent range of dimensions of the bridge decks are summarized in Table 3-1, along with other important details of the tested specimens (Okada et al. 1978; Sonoda and Horikawa 1982; Perdikaris and Beim 1988; Csagoly and Lybas 1989; Youn and Chang 1998; Graddy et al. 2002; El-Ragaby et al. 2007; Yoshitake et al. 2010; Cuelho and Stephens 2013; Tauskela 2020). It is important to notice that the different steel reinforcement ratios of the concrete bridge deck specimens may result in different failure mechanisms of the bridge deck. In general, concrete bridge decks require sufficient transverse reinforcements as tension-tie bars to develop the so-called arching action that greatly improves the load carry capacity estimated by the flexural theory (Graddy et al. 2002).

Table 3-1 Details of bridge deck specimens under fatigue loading based on the literature

Length (ft)	2.3 – 50	Width (girder spacing) (ft)	5.9 – 12.8
Thickness (in)	6.5 – 8.5	Concrete strength (psi)	3626 – 6685
Top longitudinal reinforcement ratio (%)	0.17 – 0.7	Top transverse reinforcement ratio (%)	0.2 – 0.7
Bottom longitudinal reinforcement ratio (%)	0.3 – 1.32	Bottom transverse reinforcement ratio (%)	0.23 – 1.96

Note: this table is based on 65 tested specimens, including 17 static, 32 fatigue pulsating and 16 moving fatigue specimens.

3.2.2 Test setup

The test setup of RC bridge decks under fixed pulsating load is usually the same as that of the specimens aim to obtain the static load capacity under a concentrated load. In general, the RC bridge deck specimen is casted on steel girders by means of the shear studs to reach a full composite action, as presented in Fig. 3-1. Diaphragms are placed at the ends of the bridge deck to provide support at the short edges. Interior diaphragms are also necessary for specimens with a long span to width ratio to enhance the lateral restriction of the deck. The patch load is applied by means of the hydraulic actuator connected to the reaction frame, as shown in Fig. 3-2. Neoprene or steel loading plates with a size close to the truck tire footprint is placed in between the actuator head and the top surface of the deck specimen to simulate the tire contact area in the field. During the fatigue loading process, a sinusoidal pulsating load is usually applied to the center of the tested bridge deck specimen with a frequency mostly ranges within 1–5 Hz as reported in the literatures. Although a multiple-span (more than two steel girders) specimen in transverse direction is more representative of the real bridges, most experiments only focused on the behavior of a single span bridge deck for simplicity (Okada et al. 1978; Sonoda and Horikawa 1982; Youn and Chang 1998; Bakht and Lam 2000; Graddy et al. 2002; El-Ragaby et al. 2007).

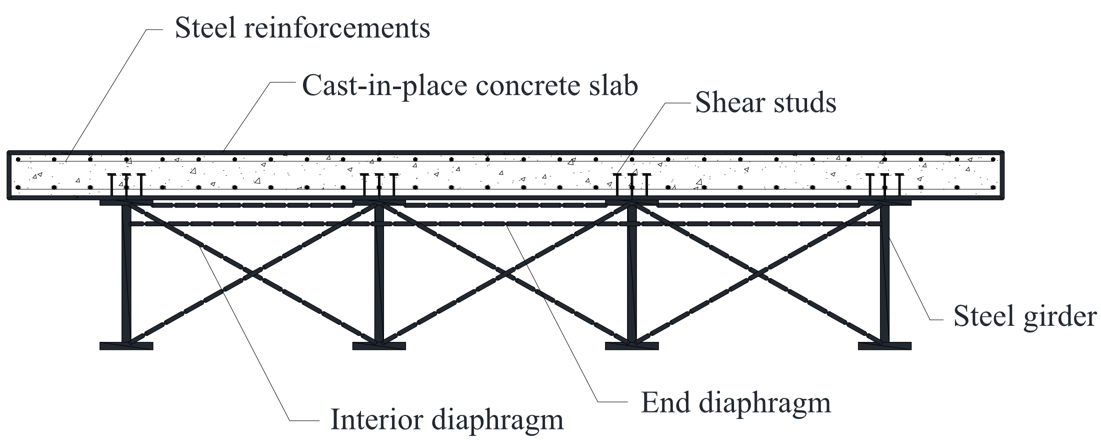

Fig. 3-1 Typical cross-section of RC bridge deck specimen (adapted from Fang et al. 1990)

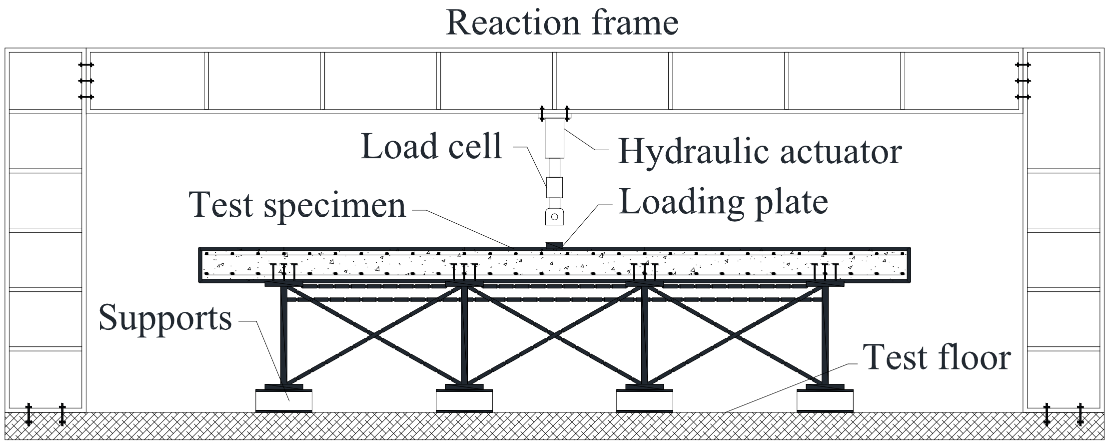

Fig. 3-2 Typical loading system for the bridge deck under a concentrated load (adapted from Youn and Chang 1998)

A more advanced loading setup is using either the moving wheels with attached hydraulic device or the pseudo-moving load strategy by changing the position of the actuator. The moving load case is more approximate to the field condition of bridge decks under daily traffic, but very few studies performed tests in this way because of the complexity of the test setup. Okada et al. (1978) carried out a moving load fatigue test on the bridge decks by sliding the slabs in the longitudinal direction and changing the supporting point of the reaction beam in the transverse direction. Likewise, Sonoda and Horikawa (1982) applied the moving load by directly changing the position of the actuator for each fatigue cycle. Perdikaris and Beim (1988) used a custom-built hydraulic cylinder attached to a steel trailer that rolls on a hardened steel plate to simulate the moving wheel load. Cuelho and Stephens (2013) adopted an advanced Automated Bridge Deck Tester (ABDT) for their full-scale bridge desk fatigue test, and the moving load is applied through a single dual-wheel assembly equipped with real truck tires, as presented in Fig. 3-3(a). Tauskela (2020) used the Rolling Load Simulator (ROLLS) to conduct the fatigue test of a full-scall concrete bridge deck with GFRP and steel reinforcement, this testing apparatus includes a steel supporting structure, the rolling load vehicle (RLV), and a high-power electric motor, as presented in Fig. 3-3(b). The speed of moving load applied to the bridge deck highly depends on the mechanical capacity of the adopted moving device, and the maximum speed varied within 1.5 – 13.1 ft/sec according to the reported tests.

(a) ABDT (Cuelho and Stephens 2013) (b) ROLLS (Tauskela 2020)

Fig. 3-3 Advanced moving load device for the fatigue test of bridge decks

3.2.3 Static test observations

Prior to the fatigue test of deck specimens, it is common to conduct a static test to examine the load carrying capacity of the deck slab and use it as a reference to determine the fatigue load range. As the applied patch load increased, the deflection of the deck increased accordingly. And the behaviors of the applied load vs. slab deflection were highly relevant to the reinforcement ratios of the tested specimens. A higher transverse reinforcement ratio usually led to a stiffer response of the specimen and a higher failure load as well (Perdikaris and Beim 1988). As presented in Fig. 3-4, the orthotropic specimen almost had a consistent linear behavior before the static failure, while the isotropic specimen performed a more non-linear response with a higher ductility at failure.

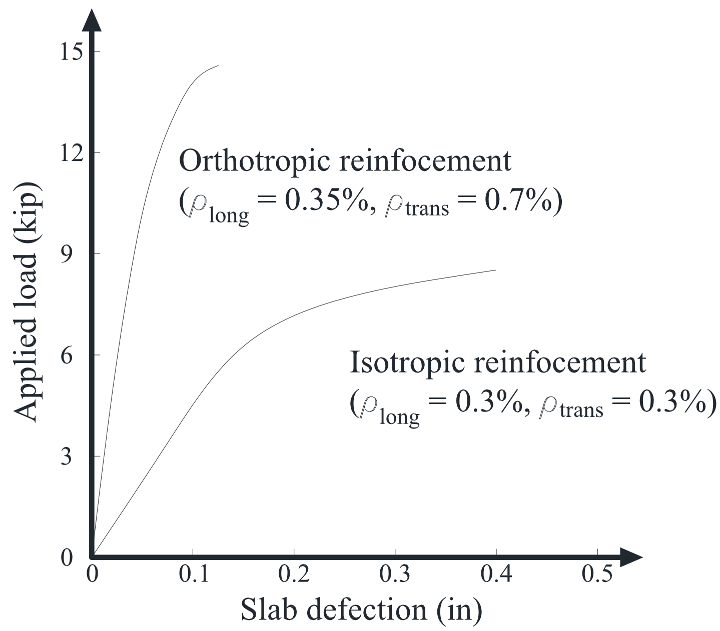

Fig. 3-4 Typical load vs. deflection behavior of bridge deck slab under static concentrated load (adapted from Perdikaris and Beim 1988)

In terms of the failure procedure, for a deck slab with a proper reinforcement ratio, with the increase of the applied load, flexural cracks of concrete occurred at the bottom of the slab beneath the loading point and then gradually propagates in both directions. Cracks developed wider with a further increase of load followed by the yielding of bottom reinforcement. In addition, concrete cracks on top of the deck slab appeared later (Sonoda and Horikawa 1982; Fang et al. 1990; El-Ragaby et al. 2007) in an elliptical form around the corners of the slab or close to the edge supports. As shown in Fig. 3-5, most tested specimens finally failed in a punching shear mode or with a flexural failure pattern to different extents, and a typical fan-shape cracking pattern was often observed. The shape and size of the local punched-in concrete area on top surface of the deck was usually similar to that of the loading plate.

It should also be noted that the failure modes highly depend on the boundary conditions of the slab and the reinforcement ratio. For example, the unreinforced specimens tested by Perdikaris and Beim (1988) failed in flexural mode, while all the other reinforced specimens failed in a punching shear mode. Sonoda and Horikawa (1982) reported a partially flexural failure in addition to the punching shear collapse of the deck slab, because the specimens were simply supported with no restrictions of the rotation at the slab edges.

By contrast, the deck specimens of Youn and Chang (1998) and Fang et al. (1990) used the shear studs welded on the steel girders to reach the full composite action. The rigid connection between the cast-in-place concrete deck slab and the supporting girders ensured the internal arching development of the concrete and thus all specimens failed by punching shear. Furthermore, the steel-free deck slabs tested by Bakht and Lam (2000) had the failure modes of either punching shear, or bending; or a mixed mode of bending and punching shear, depending on the different transverse confining systems that adopted.

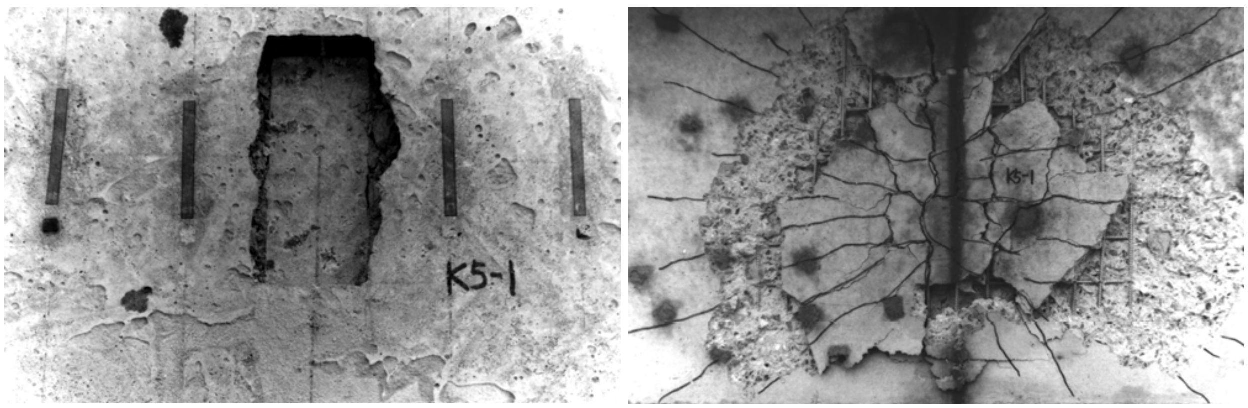

(a) top surface (b) bottom surface

Fig. 3-5 Cracking pattern of punching shear failure of the bridge deck slab (Youn and Chang 1998)

3.2.4 Fatigue test observations

The fatigue behavior of concrete deck slab under cyclic loading varies depending on the different fatigue loading scheme. As mentioned above, most tests used the pulsating load applied to a fixed position of the tested slab with either a constant or changing fatigue load range. For example, Okada et al. (1978) and El-Ragaby et al. (2007) both adopted a stepwise fatigue loading strategy to speed up the fatigue degradation of deck slabs to reach failure. While others set the peak fatigue load as a fixed percentage ratio with respect the static ultimate strength of the slab, and it varied within the range of approximately 50 – 90% (Sonoda and Horikawa 1982; Perdikaris and Beim 1988; Youn and Chang 1998; Graddy et al. 2002).

Regardless of the different loading strategy and specimen details, the fatigue behaviors of the tested deck slabs have many similarities. As presented in Fig. 3-6, all the deck specimens exhibited a gradual increase in deflection at the loaded point with the increase of fatigue cycles, and it also resulted in a stiffness loss to different extent. The variation in stiffness loss may be contributed by the difference in percentage ratios of reinforcement, type of reinforcement, fatigue load range and scatter of concrete material, etc. Meanwhile, the tensile strains of the bottom reinforcements in transverse direction gradually increased because of the concrete degradation under fatigue loading (Okada et al. 1978; Youn and Chang 1998; El-Ragaby et al. 2007). However, this tendency is not always true for the deck slab with a high percentage ratio of transverse reinforcement. Perdikaris and Beim (1988) reported that the measured tensile strain of the transverse reinforcement did not change after 160,000 cycles for the orthotropic deck specimen. Test results of Sonoda and Horikawa (1982) even indicated a decrease of the transverse reinforcement strain during fatigue cycles, and it was possibly due to the redistribution of stresses resulting from both the internal bond slips of reinforcements and the orthotropy of the flexural rigidity of the slabs. Moreover, the increase of the transverse concrete compressive strain at the top deck surface was observed with the increase of fatigue cycles (El-Ragaby et al. 2007).

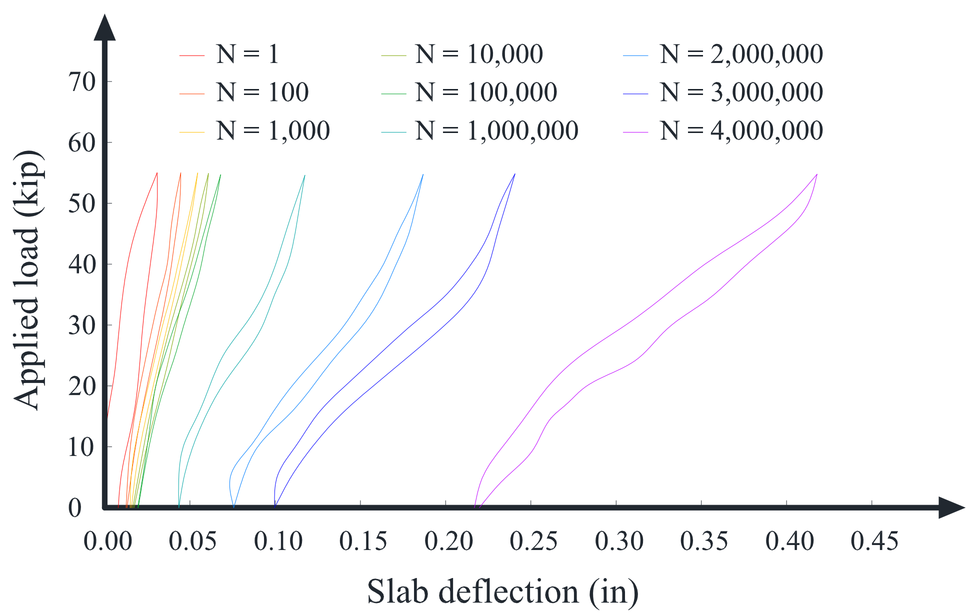

Fig. 3-6 Typical slab deflections during the fatigue cycles (adapted from Graddy et al. 2002)

The failure process of bridge deck specimen under fatigue loading is very similar to that of the static case. Flexural cracks of concrete usually occurred firstly at the bottom of the pulsating load position, and it grew wider and spread to a larger circular area as the number of fatigue cycles increased. When the specimen reached a relative stable condition, the crack growth reduced considerably but the crack width continued to increase (Youn and Chang 1998). Aggregate debris or even pieces of concrete might drop from the bottom slab when large concrete cracks formed (Graddy et al. 2002; El-Ragaby et al. 2007). Finally, the deck slab failed in a fan-shape punching shear mode.

For tested specimens under moving wheels or pseudo-moving fatigue loading, the fatigue life significantly drops compared to those pulsating loading cases at fixed positions. Sonoda and Horikawa (1982) reported that the fatigue life of deck specimen under wheel loading could be shorten as much as two orders of magnitude. Likewise, from the test results of specimens subjected to moving wheel load, Perdikaris and Beim (1988) concluded that one wheel load passage is equivalent in damage to about 34 and 1800 load cycles of the pulsating load for the isotropic and orthotropic bridge deck, respectively. On the other hand, because of the longitudinal movement of the wheel load, the entire deck reinforcements were stressed in contrast to the pulsating loading case where only the reinforcement in the vicinity of the loading point was affect. As a result, cracks at the bottom of the deck slab developed transversely along the entire deck length and formed a unique grid-like cracking pattern, as presented in Fig. 3-7. This cracking pattern was confirmed by Cuelho and Stephens (2013) in their full-scale bridge deck fatigue test under the real truck tires. The alternating crack opening-closing and twisting of the faces of the orthogonal crack as the wheel load moved on the deck significantly accelerated the concrete deterioration and debonding at the interface between concrete and reinforcements, and eventually led to a punching-type failure of the deck (Perdikaris and Beim 1988). This failure mechanism was also observed in the pseudo-moving fatigue test conducted by Okada et al. (1978).

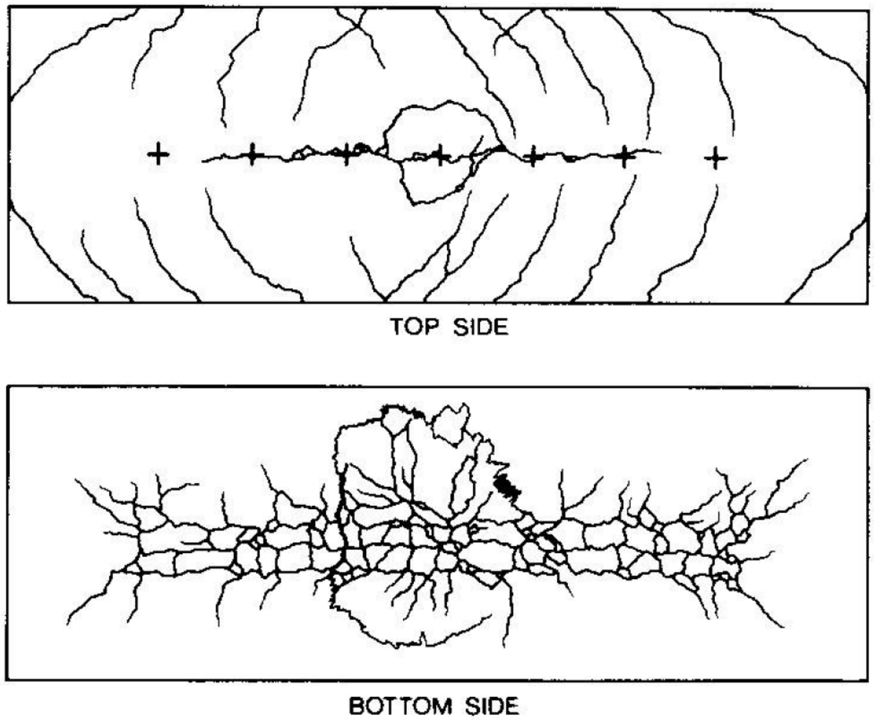

Fig. 3-7 Typical cracking pattern of bridge deck slab under moving wheel load (Sonoda and Horikawa 1982)

3.3 Models and analytical study

To fully understand the punching shear failure mechanism of bridge deck under both static and different fatigue loading scenarios, and to well explain the internal arching action, analytical efforts have been made by different studies. Most adopted models focus on the punching shear failure mechanism of the deck slab under a concentrated load for the static case. And the yield line theory has also been used to estimate the ultimate strength of the deck as an upper bound. In addition, a few studies investigate the failure procedure of RC bridge deck by means of the numerical models, as well as the degradation behaviors under cyclic loading case. However, the primary method to estimate the fatigue life of bridge deck specimens is still through the semi-empirical models calibrated from the test data points. This section will focus on both the analytical and semi-empirical methodologies that are popular in the literatures to estimate the load carrying capacity and fatigue life of RC bridge decks.

3.3.1 Punching shear models

As aforementioned in section 3.2.3, the typical failure mode observed in the experiments is the fan-shape punching shear. The idealized model can be illustrated as Fig. 3-8, where the concrete wedges bound by the shear cracks act as rigid bodies in the radial direction and rotate about the center of rotation (CR). Due to the cracking of concrete, the neutral axis of the slab migrates toward the top surface at the mid span and its position varies along the span of the slab. Meanwhile, the boundary of the slab restricts the rotation tendency of the wedge element which result in the compressive membrane action or the arching force in the RC deck slab [Fig. 3-8(b)]. This arching action will significantly enhance the load carrying capacity of the slab.

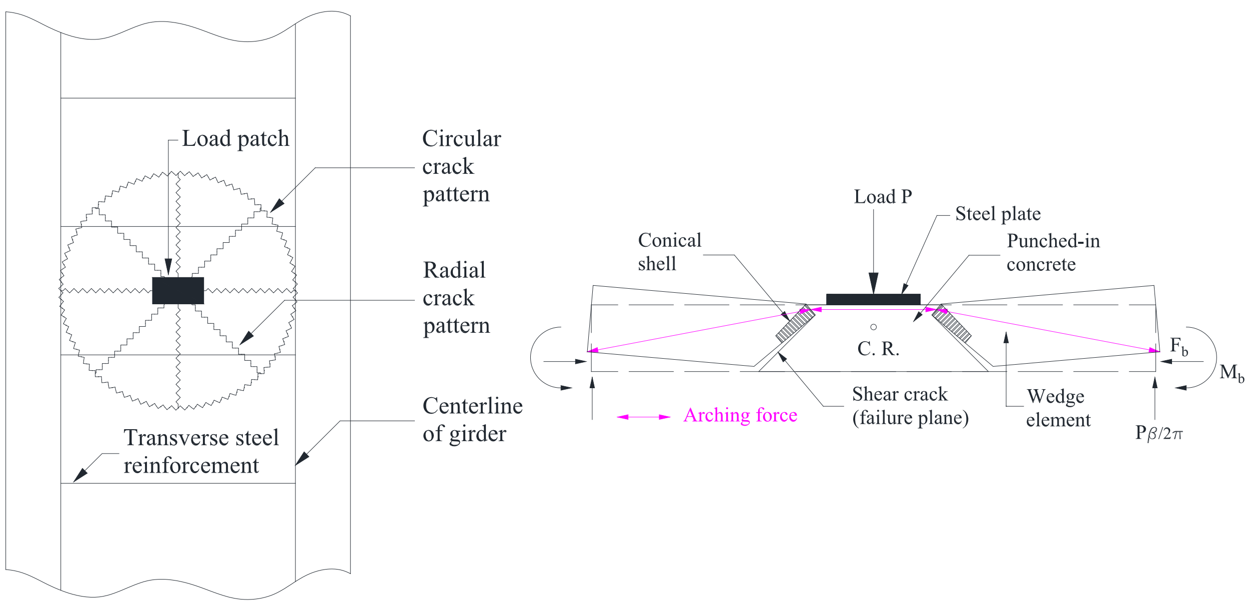

(a) Fan-shape cracking pattern (b) Rigid body rotation of cracked concrete wedges

Fig. 3-8 Idealized punching shear failure of concrete slab under a concentrated load (adapted from Hewitt and Batchelor 1975 and Mufti and Newhook 1998)

If it is assumed that only the concrete tensile stress exists at the failure plane, then the trapezoidal punched-in concrete can be isolated as a single rigid body to estimate the punching shear capacity. As presented in Fig. 3-9, a simple general punching shear model is thus introduced to estimate the theoretical punching shear capacity of bridge deck (Fang et al. 1990). In Fig. 3-9(a), the concentrated load footprint is assumed as a rectangular shape with the size of $b_1 \times b_2$, and the failure planes have the same inclination angle θ. The failure plane propagates downward to the bottom of the deck slab by a thickness of d. Fig. 3-9(b) illustrates the free-body diagram of the failure plane under applied forces, hence, the punching shear capacity can be easily derived from the equilibrium of these forces as:

$$V_c = 2\left(b_1 + b_2 + \frac{2d}{tan\theta}\right)\frac{d}{tan\theta}f_t \tag{3.1}$$

where b_1 = long side of tire footprint (in); and b_2 = short side of tire footprint (in). And the tensile strength of concrete on the failure plane can be referred to ACI 318 Table 22.6.5.2 (ACI 2019) as

$$f_t = (2 + \tfrac{4}{\beta})\lambda_s\lambda\sqrt{f_c'} \leq 4\lambda_s\lambda\sqrt{f_c'} \tag{3.2}$$

where λ_s = size effect factor = $\sqrt{2/(1 + d/10)} \leq 1$; λ = modification factor of lightweight concrete; β = ratio of long to short side of the tire footprint; and f_c' = concrete compressive strength (psi).

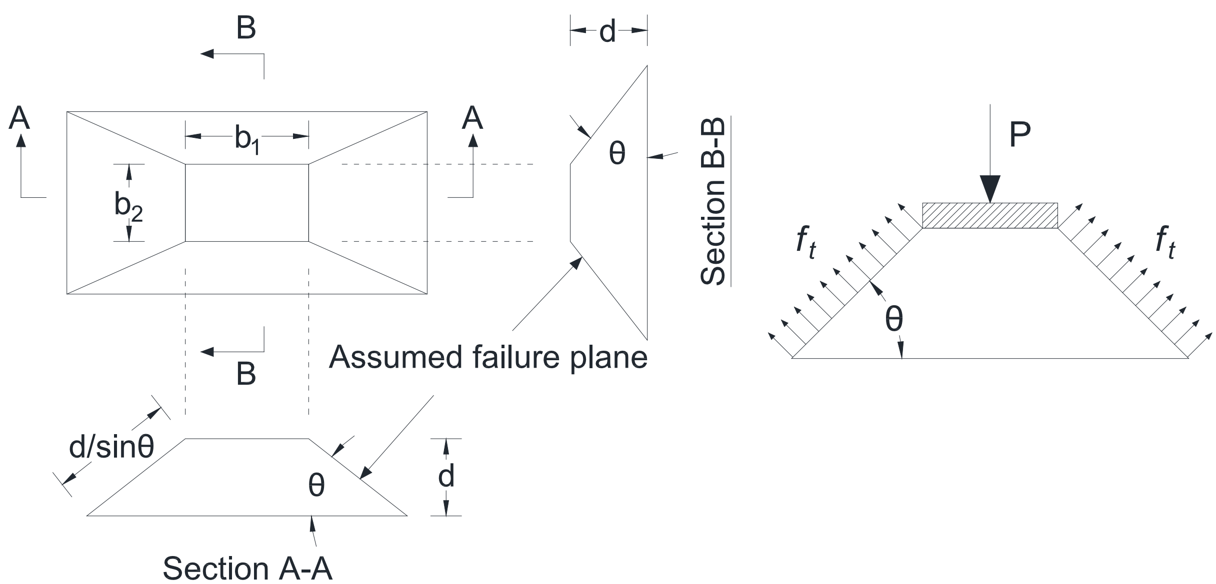

(a) Assumed failure plane in punching shear (b) Forces acting on the failure plane

Fig. 3-9 General punching shear model (adapted from Graddy et al. 2002)

However, despite its simplicity and popularity in design and research, this general punching shear model does not quantify the influence of arching force, neither does it incorporate the contribution from reinforcements. Alternatively, another fatigue punching shear model proposed by Matsui (1991) considers the influence of both compressive and tensile reinforcements at the ultimate state of the deck slab. The formation of the fatigue punching shear model proposed by Matsui is described as below:

$$P_{sf} = 2B(\tau_{s,max}X_m + \sigma_{t,max}C_m) \tag{3.3}$$

$$B = b + 2d_b \tag{3.4}$$

$$\tau_{s,max} = 0.688 f_c'^{0.61} \leq f_c' = 80\ MPa \tag{3.5}$$

$$\sigma_{t,max} = 0.269 f_c'^{2/3} \tag{3.6}$$

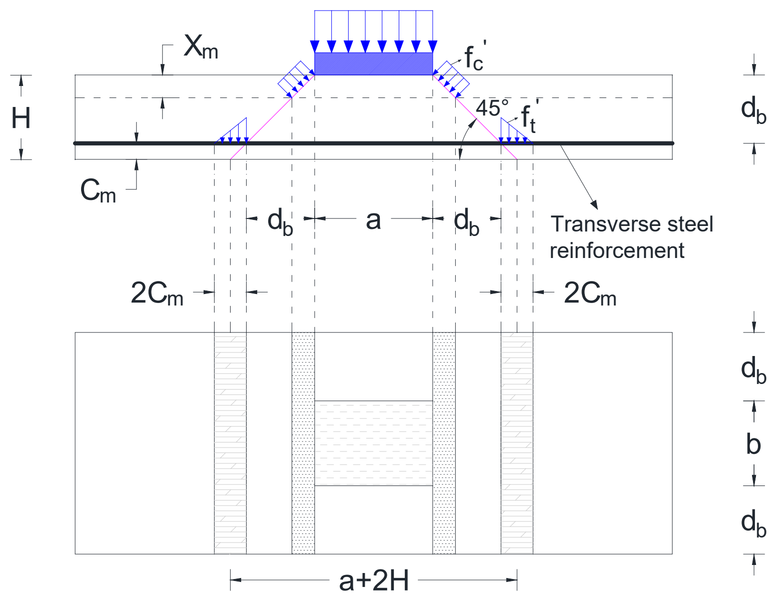

Fig. 3-10 The fatigue punching shear model proposed by Matsui (1991)

where B = effective width of the RC bridge deck slab (mm), a = contact length of tire in the transverse direction of bridge (mm) = 2.5b; b = contact width of tire in the longitudinal direction of bridge (mm); H = RC bridge deck thickness (mm); d_b = effective depth of transverse reinforcement at the tension side (mm); f_c' = concrete compressive stress at the failure plane (MPa); f_t' = tensile stress at the failure plane (MPa); $\tau_{s,max}$ = maximum shear strength of concrete (MPa); $\sigma_{t,max}$ = maximum tensile strength of concrete (MPa); X_m = depth of neutral axis (mm); and C_m = cover depth at the tension side (mm), as illustrated Fig. 3-10. It should be noted that the original unit system for this model is in metric, hence, both the maximum shear strength and the maximum tensile strength of concrete need to be converted from psi for consistency to yield the punching shear capacity in newtons. However, to accommodate the fatigue life model proposed by Matsui (1991) which will be introduced later, this fatigue punching shear model only includes the contribution from two transverse faces out of the representative four punching shear failure faces, as observed in most experiments (Fig. 3-5). As a result, a more conservative estimation of the punching shear capacity using this model should be expected.

On the other hand, more advanced models have also been developed for the punching shear failure of bridge deck slabs and incorporate the arching force into the prediction. For example, Hewitt and Batchelor (1975) extended the model of Kinnunen and Nylander (1960) by incorporating the influence of different boundary restrictions via the restraining force F_b and moment M_b, as shown in Fig. 3-8(b) where β represents the angle of wedge element (sector). Instead of using the punched-in concrete portion, the cracked concrete wedge is focused, and all the forces applied to the wedge are considered, including the compression forces of concrete (e.g., internal arching), forces in the circumferential reinforcement and boundary reactions. In addition, a restraining factor F_R was introduced to quantify the degree of boundary conditions, and it varies within 0–1.0, with 0 represents the simply supported case and the latter represents the ideal infinitely rigid condition. The failure criterion is that punching occurs when the tangential strain at the top of the slab in the vicinity of the root of the shear crack (conical shell) reaches a critical value. A dowel factor equals to 1.2 is included in this model as well to consider the enhancement of deck slab from two-way reinforcements. However, iteration process by computer program is inevitable to determine the punching load with the given failure criterion. Likewise, Mufti and Newhook (1998) adopted a similar methodology by solving the equilibrium state of forces applying to the wedge element but did not include the restraining moment contributed by the boundary conditions. They also took the triaxial compressive state of the conical shell into consideration to estimate a more realistic ultimate concrete strength at failure.

3.3.2 Yield line theory

Due to the predominant failure mode of punching shear for tested deck slabs under the concentrated load, it can be inferred that the actual flexural capacity of the deck slab is larger than its punching shear capacity. The yield line theory, which measures the ultimate flexural strength of a supported slab in the most ideal situation, is usually adopted to predict the upper bound failure loads of the slabs with different boundary conditions. Analytical results from Fang et al. (1990) and Graddy et al. (2002) both confirmed the overestimation of the yield line theory to predict the load carrying capacity of tested deck specimens. However, Sonoda and Horikawa (1982) reported a very close estimation of the failure load compared to the test results by using the yield line theory. Regardless of the discrepancy in the accuracy of predicted failure loads, it is beneficial to introduce the concept of yield line theory as an alternative to the punching shear models.

The yield line is defined as a crack in a reinforced concrete slab across which the reinforcing bars have yield and along which plastic rotation occurs (Kennedy and Goodchild 2004). For example, if a deck slab is supported between girders, the yield line pattern may be represented by the illustrations as show in Fig. 3-11. In either case, i.e., two way or one way action, the yield lines depict the boundaries between different rigid regions. These regions rotate about the yield lines, as well as pivot about the axes of rotation which usually locate close to the line of support. Assuming the rigid region rotate an angle of θ_i about its axis of rotation, and the vertical displacement at the loading point equals to δ, then an equilibrium equation in terms of energy can be reached. In other words, the work done by the external load equals to the dissipated energy by rotations about yield lines as below:

$$P\delta = \sum_{i=1}^{n} m_i \, l_i \theta_i \tag{3.7}$$

where P = concentrated load applied to the deck slab; m_i = moment resistance of the slab per unit length at the i^{th} yield line; and l_i = the length of the i^{th} yield line or its projected length onto the axis of rotation of that region. The moment resistance m_i at each yield line can be calculated by using the actual material properties through the classic beam theory. And the rotation angle θ_i can be presented in terms of δ using the geometrical relationship between different rigid regions. Thus, the load carrying capacity of the deck slab can be obtained by solving the Eq. (3.7).

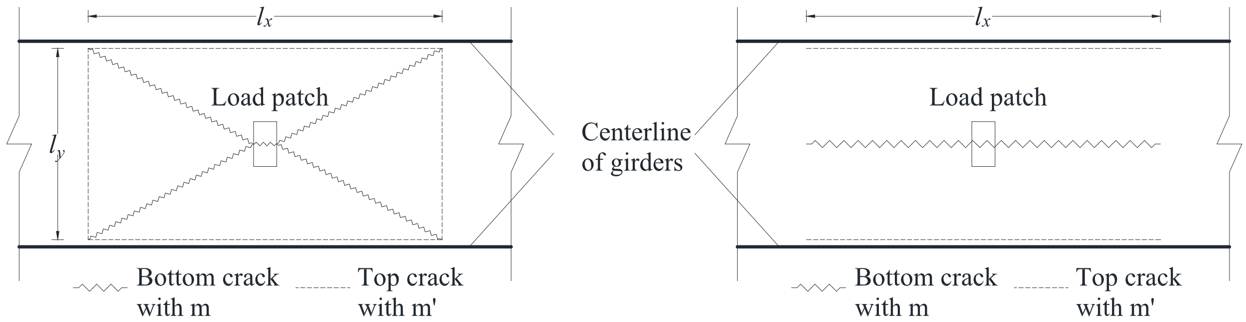

(a) Two-way action (b) One -way action

Fig. 3-11 Potential yield line patterns of deck slab under patch load case (adapted from Fang et al. 1990)

However, it should be noted that the yield line pattern needs to be predetermined to formulate the energy equilibrium equation. As a result, the predicted load carrying capacity depends on the selected cracking pattern. And it is possible that the deck slab has various failure pattern corresponding to different failure loads. Kennedy and Goodchild (2004) also recommended a 10% margin on the design load by using the yield line theory to allow for the effects of corner levers in two-way slabs.

3.3.3 Fatigue life models

The fatigue life of RC bridge deck is usually interpretated by a logarithmic relationship with the applied load level P/P_s, or the shear stress level v/v_c, where P = maximum fatigue load applied to the deck slab; P_s = static failure load of the deck slab obtained from test; v = nominal punching shear stress acting on the failure plane; and v_c = shear strength of the concrete. Because the failure of bridge deck under cyclic loads is highly relevant to the degradation of concrete material, thus, its fatigue characteristics shares many similarities with the fatigue of plain concrete. In other words, scatter is inevitable in the fatigue life of identical bridge deck specimens subjected to the same loading condition, and it has been confirmed by experimental studies (Perdikaris and Beim 1988; Youn and Chang 1998; Graddy et al. 2002). To this end, a large database of test results is necessary to yield a reliable fatigue life model. However, due to the limited number of fatigue tests on the deck slabs, the proposed fatigue life models in the literatures so far are barely satisfying to accommodate to different deck specimens. And neither of these models considers the influence due to loading frequency and duration or discrepancy in material properties. Nevertheless, these models are still presented herein as references.

(1) *Model of Sonoda and Horikawa (1982)*

Sonoda and Horikawa (1982) tested RC deck slabs with either isotropic or orthotropic reinforcement arrangement, subjected to both fixed pulsating and pseudo-moving loading cases. The total number of deck slabs is 20 with a selected fatigue load levels ranging from 50 – 85% with respect to the static load carrying capacity. The fatigue life model was proposed with an upper bound of load cycles equals to two million as below:

$$\frac{P}{P_s} = 1.08 - 0.086 logN_f \quad \text{for isotropic slabs under fixed pulsating loading} \quad (3.8)$$

$$\frac{P}{P_s} = 1.14 - 0.093 logN_f \quad \text{for orthotropic slabs under fixed pulsating loading} \quad (3.9)$$

$$\frac{P}{P_s} = 0.93 - 0.076 logN_f \quad \text{for isotropic slabs under moving loading} \quad (3.10)$$

$$\frac{P}{P_s} = 0.99 - 0.102 logN_f \quad \text{for orthotropic slabs under moving loading} \quad (3.11)$$

(2) *Model of Matsui (1991)*

Matsui (1991) (as referenced by Yoshitake et al. 2010) proposed a semi-empirical equation to estimate the fatigue life of RC deck slabs subjected to moving wheel load as below:

$$log\left(\frac{P}{P_{sf}}\right) = -0.07835 logN_f + logC \quad (3.12)$$

where P_{sf} = fatigue punching shear capacity as introduced in section 3.3.1 and C = service coefficient equals to 1.23 and 1.52 for wet and dry conditions, respectively. This equation is only valid for N_f greater than 10,000 cycles.

(3) *Model of Youn and Chang (1998)*

Youn and Chang (1998) conducted both the static and fixed pulsating tests at the different positions of the deck slabs. Although they applied a fixed peak fatigue load level of either 59% or 65% based on the average punching shear strength obtained from the static test, the fatigue model is calibrated from the actual load percentage ratio with respect to the various punching shear strengths at different loading positions. They concluded an endurance limit of $0.55P_s$ to reach the recommended fatigue life of 2 million cycles, and the model is presented as follows:

$$log\left(\frac{P}{P_s}\right) = -0.066logN_f + log1.4461 \tag{3.13}$$

(4) *Model of El-Ragaby et al. (2007)*

El-Ragaby et al. (2007) tested five full-scale deck slabs reinforced with either GFRP or steel reinforcements under a stepwise fatigue loading scheme with an increasing peak fatigue load. To extend the database, the PM rule (as introduced in section 2.3.6) was adopted to obtain the equivalent fatigue life of specimens under different peak fatigue loads. A parabolic semi-logarithmic function based on the model of Matsui (1991) was proposed through regression analysis to include the characteristics of fatigue life pattern under higher fatigue load levels as well as follows:

$$\frac{P}{P_s} = 0.0034\left(logN_f\right)^2 - 0.11873\left(logN_f\right) + 1.0752 \tag{3.14}$$

3.3.4 Finite element simulation

The full-scale fatigue tests of RC bridge decks are usually complicated, time consuming and expensive, let alone a large database is always necessary to propose a reliable fatigue model. As an alternative to the experiment, numerical studies have also been made on the simulation of deck slabs subjected to fatigue loading by means of the finite element method (FEM). Some of the representative research is presented in this section.

For example, Maekawa et al. (2006a) extended the direct path-integral scheme (Maekawa et al. 2006b) to the full three-dimensional (3D) analysis of fatigue failure and applied this method to the fatigue life simulation of RC decks subjected to moving wheel loads. A computational constitutive model of concrete was used to consider the effect of concrete degradation due to crack development, time-dependent elastoplastic fracture, and fatigue damage (Maekawa and El-Kashif 2004). In addition, a 3D multi-directional non-orthogonal fixed crack approach was proposed for the fatigue simulation by using the composition method (Maekawa et al. 2003). In this study, a simply supported RC deck slab was modeled representing the tested specimen from Maeda and Matsui (1984) under moving wheel loads, as presented in Fig. 3-12. The analysis indicated a significant decrease of fatigue life in two or three order of magnitudes for the case under the moving wheel loads compared to the fixed pulsating case. The results of sensitivity study also inferred that the predominant factors in fatigue degradation of RC deck slab are the shear transfer fatigue along cracks, and the bond decay (tension-stiffness). Moreover, the effect of boundary conditions was investigated, and it confirmed that the fixed translational boundary can increase the slab fatigue life compared to the free translational boundary.

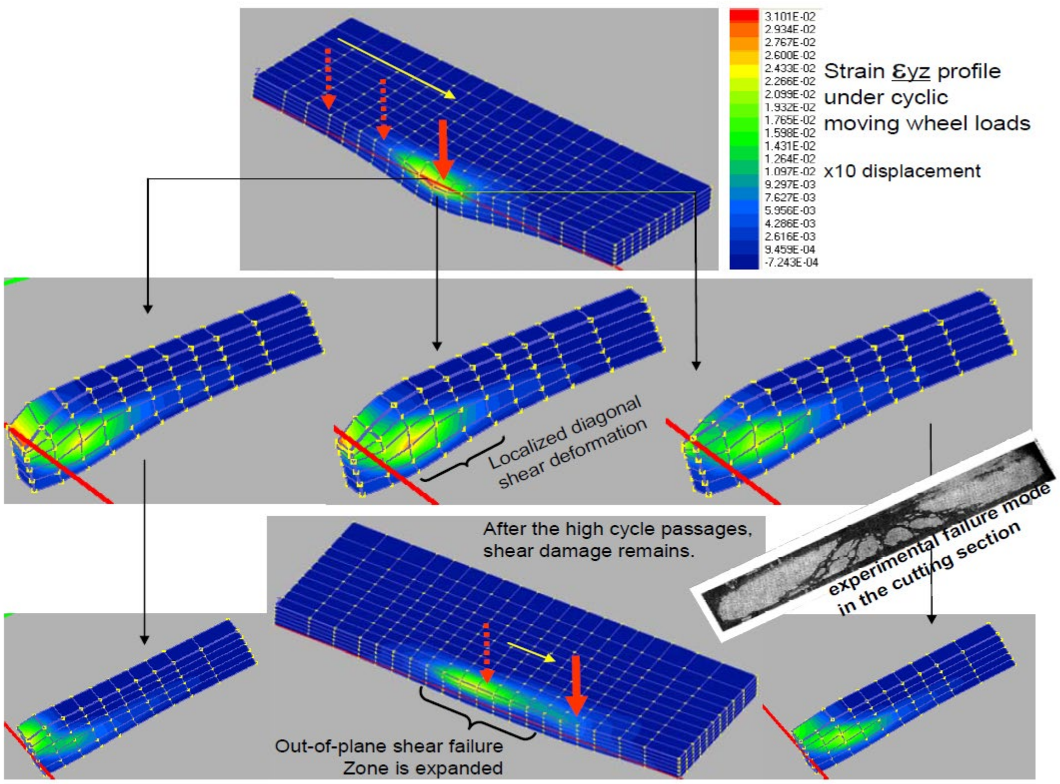

Fig. 3-12 Visualized FE results of transverse (magnified) deformation of RC deck slab under moving wheel load (Maekawa et al. 2006a)

Suthiwarapirak and Matsumoto (2006) constructed a FE model of the bridge deck slab based on the experiment of Okada et al. (1978). The concept of crack bridging degradation was adopted to explain the crack initiation and propagation of concrete during cyclic loading, which leads to the fatigue failure of the deck slab. The concrete smeared crack element with a multiple fixed crack concept was used to represent the cementitious material and the rod element with a bilinear stress-strain relationship was used to represent the steel reinforcement. This model successfully reproduced the crack development and damage accumulation of the concrete material and can estimate the fatigue life of the deck slab, as illustrated in Fig. 3-13. However, it overestimated the fatigue life of deck slab subjected to moving wheel loads. This overestimation is probably caused by the model assumptions that both the fatigue degradation of the shear stress and the bond degradation between the reinforcement and concrete were not considered in the numerical simulation.

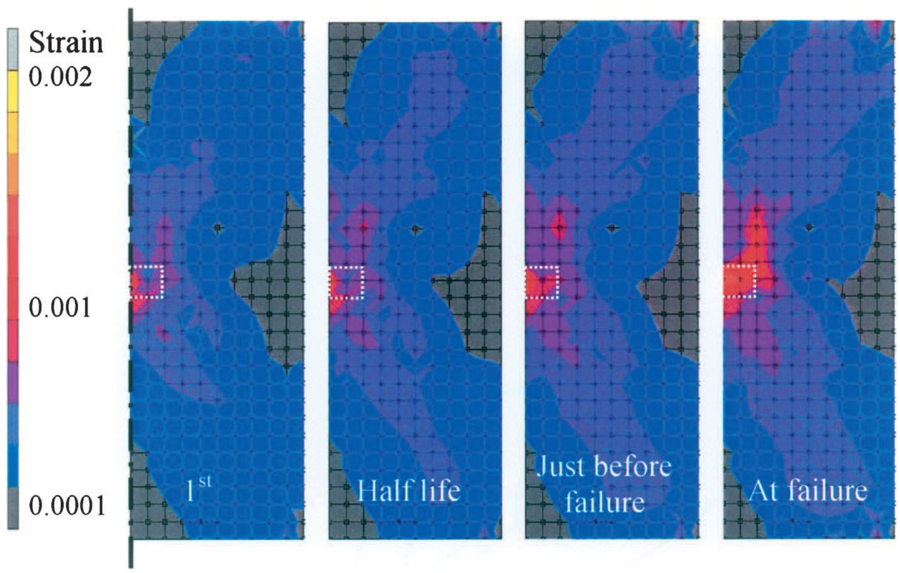

Fig. 3-13 Damage accumulation at the bottom of the deck slab during fatigue cycles (Suthiwarapirak and Matsumoto 2006)

Moreover, Drar and Matsumoto (2016) extended the FE modeling strategy of Suthiwarapirak and Matsumoto (2006) by incorporating the bond-slip effect between the reinforcing bar and the surround concrete. RC deck slabs were modeled referring to the experiments conducted by Shakushiro et al. (2011) with either deformed bars or plain bars. The numerical simulation reached a good agreement with the test results, in terms of slab displacement vs. number of fatigue cycles, fatigue life, cracking pattern and strain development of steel reinforcements. A typical comparison between the predicted cracking patterns at the bottom of the RC deck slab and the test observations is presented in Fig. 3-14. In addition, all the analyzed slab models failed in a punching shear mode with an inner cracking orientation of 45°in the transverse direction, which was consistent with the test results. The FE model analysis also indicated that the RC deck slab reinforced with plain bars has a larger displacement and a shorter fatigue life than that reinforced with deformed bars.

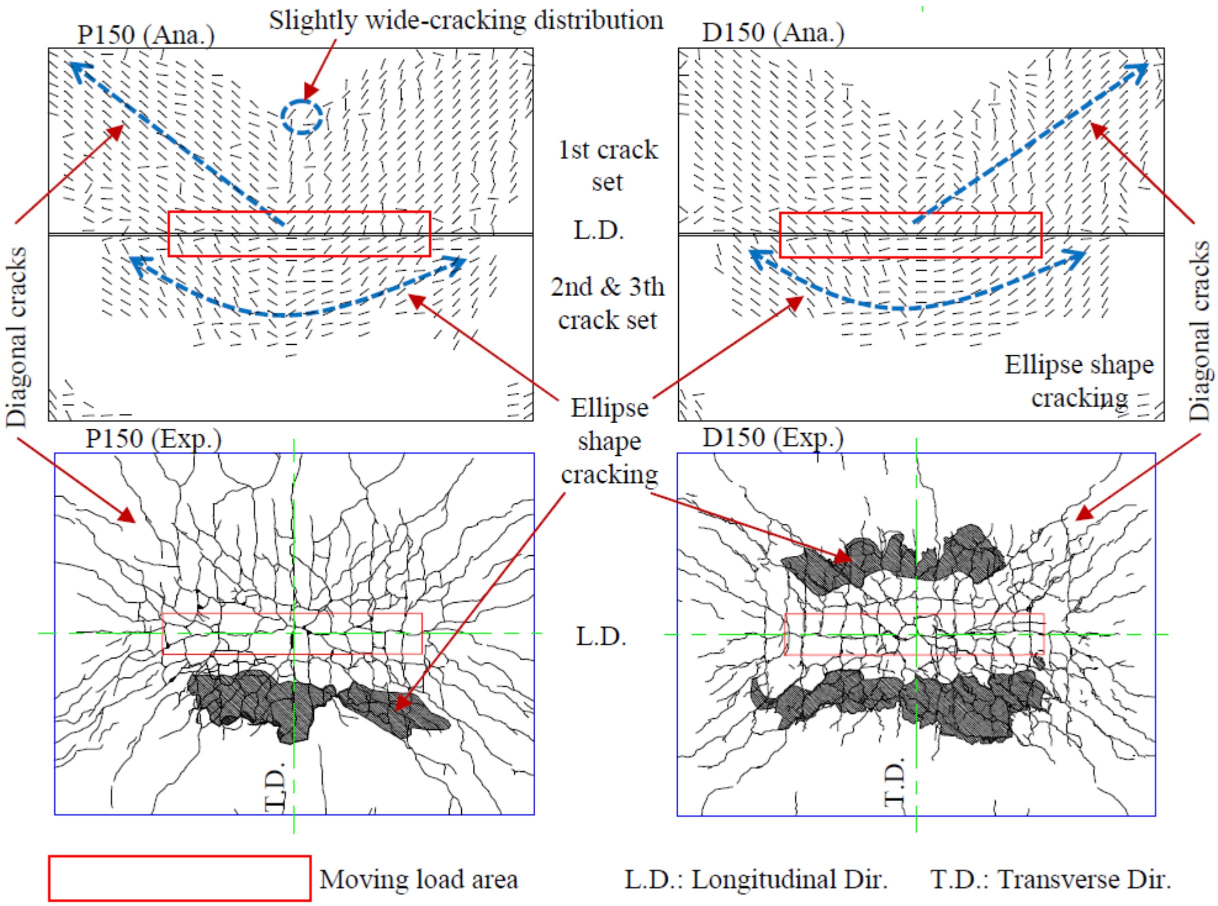

Fig. 3-14 Cracking patterns at the bottom of the RC deck slab at the failure load (Drar and Matsumoto 2016)

4 CONCLUSIONS AND RECOMMENDATIONS

4.1 Conclusions

A thorough state-of-the-art literature review on the fatigue behavior of reinforced concrete bridge deck is presented in this report, including both the material and structural level. For plain concrete subjected to cyclic loading, the internal damage accumulates due to the applied load loops in terms of the dissipated energy. With a constant fatigue stress range, the material properties of concrete gradually degrade, including a declining tendency of concrete strength and stiffness, accompanied by an increase in the permanent concrete strain. It is believed that the major factors contributed to the fatigue life of concrete include, but not limited to, the normalized stress level, stress reversal, lateral confinement, concrete creep, loading frequency, loading duration, shape of cyclic loading form and loading history. A normalized stress level of $S_{max} > 0.75$ is critical for the concrete material since it approaches the long-term strength of concrete, at which the effect of loading frequency is also more significant. In addition, the sustained loading effect on the fatigue performance of concrete is not negligible for a stress ratio $R>0.75$. Furthermore, representative concrete fatigue models are reviewed and categorized by different methodologies, which includes the deterministic model, the probabilistic model, and the energy model. These models can be adopted as good references for the fatigue design of RC bridge decks if a stress-based approach is focused.

At the structural level, both experimental and analytical studies on the fatigue characteristics of RC bridge decks are summarized. In general, RC deck slab subjected to cyclic loading has a gradual increase in the deflection at the patch load point, accompanied by a decrease in the deck stiffness. The degradation behavior of the RC deck slab is primarily caused by the accumulated damage in concrete closer to the loading position, where cracks occur and propagate in both longitudinal and transverse directions. A typical punching shear failure mode is usually observed with a fan-shape cracking pattern for fixed pulsating load or grid-like cracking pattern for moving wheel load. Due to the limited number of research effort, as well as the complex failure mechanism of bridge deck, a simple yet reliable model for the fatigue design of RC bridge decks is still lacking. Nevertheless, the existing representative models are still summarized based on either the punching shear failure mechanism with/without arching action, or the yield line theory. The force-based semi-empirical models are also collected from the literature to predict the fatigue life of RC deck slabs, although these models are only based on a very small test database. Moreover, some of the FE modeling strategies are introduced to analyze the fatigue behavior of bridge decks under cyclic loading, as an alternative to the experimental method. These numerical simulations require complex modeling and material definitions, as well as huge computational efforts to yield reliable results. However, the numerical method still deserves more investigation in the future since it helps understand the failure mechanism of bridge decks subjected to fatigue loading, and it can also extend the current test database.

4.2 Recommendations

Based on the literature review as described above, there is no doubt that the fatigue process of reinforced concrete bridge decks subjected to cyclic loading is complicated. The fatigue failure is the result comprehensively influenced by multiply factors such as damage accumulation of concrete through microcracks, triaxial compressive stress state within the internal arching, stress redistribution between concrete and steel reinforcements, restriction stiffness of deck supports, type of service load (e.g., stationary or moving load), and loading duration, etc. The proposed fatigue models of plain concrete are still debatable and require the probability theory to consider the scattering of fatigue life in general. In addition, the environmental exposure of bridge decks may significantly affect their fatigue life through the deterioration of materials, e.g., freeze and thaw cycles, corrosion due to deicing salt, aging, etc. As a result, the fatigue models of RC bridge deck reviewed in this review are far from being applicable and practical in deck fatigue design. However, they do provide important insights for the expected fatigue life of bridge deck if the on-site fatigue test is not available. Derived from the current literature review, two frameworks of methodology can be considered in the subsequent research to estimate the fatigue life of RC bridge deck based on these models:

1. *Stress-based method*: Calculate the concrete stress level S_{max} under the critical vehicle load on the failure plane of the punching shear model (Fig. 3-9), using either analytical or numerical method,

and estimate the fatigue life of bridge deck using the models introduced in section 2.4. A possible but not exclusive framework of this approach can be illustrated in Fig. 4-1.

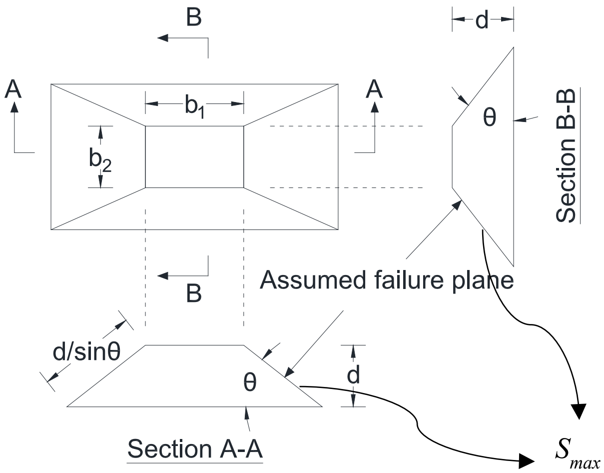

Calculate the maximum concrete stress S_{max} under the repeated vehicle load at the assumed failure plane, e.g., as shown in the left figure, using either analytical or numerical method

When S_{max} is determined, the fatigue life of this local structural component can be estimated by the existing models. For example, the most widely adopted deterministic model proposed by Hsu (1981) can be a possible choice in this case, as presented below:

$$S_{max} = 1 - 0.0662(1 - 0.556R)logN_f - 0.294logt$$

Fig. 4-1 Example framework of the stress-based method

However, this stress-based method can be extremely conservative since the stress redistribution, internal arching, and reinforcement of the deck slab are not considered. A more appropriate alternative is using these concrete fatigue models as material input to conduct an independent FE analysis, as described in section 3.3.4, followed by the definition of an appropriate failure criteria, e.g., either load-controlled failure, or deformation-controlled failure, and then estimate the fatigue life of the entire deck structure.

2. *Force-based method*: Calculate the static load carrying capacity P_s of bridge deck using either the punching shear model (section 3.3.1) or the yield line theory (section 3.3.2). Calculate the critical vehicle load P applied to the bridge deck and estimate its fatigue life using the models introduced

in section 3.3.3. A possible but not exclusive framework of this approach can be illustrated in Fig. 4-2.

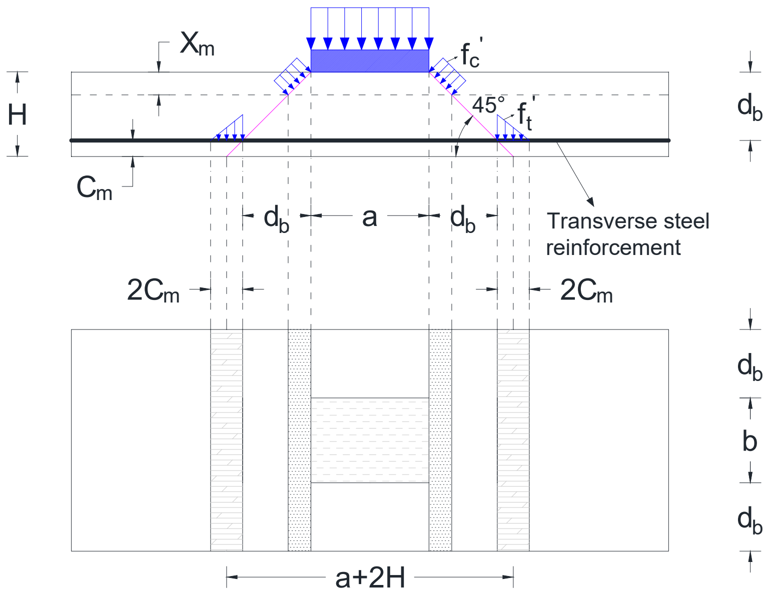

The model of Matsui (1991) as introduced in section 3.3.1, for example, is an appropriate approach to estimate the fatigue punching shear capacity P_{sf} of RC bridge deck, by incorporating the contribution from two transverse failure planes (as shown in the figure above). When P_{sf} is determined, the fatigue life of the deck can be predicted by the semi-empirical fatigue model proposed by Matsui (1991) as well in the following:

$$log\left(\frac{P}{P_s}\right) = -0.07835logN_f + logC$$

Fig. 4-2 Example framework of the force-based method

The accuracy of the force-based method highly depends on the selection of the model to estimate the local static load carrying capacity P_s, and its corresponding semi-empirical fatigue model. A tryout case study was conducted to investigate the difference in the required RC bridge deck thickness using the different static and fatigue model combinations, as described in the Appendix. A short observation of the tryout case study contains: (1) the adoption of both the static model and fatigue model of Matsui (1991), i.e., case S1F1, yields a minimum deck thickness of 7.5 in to achieve the target service life of 75 years; and

(2) the adoption of the general punching shear model (Graddy et al. 2002) and the fatigue model of El-Ragaby et al. (2007), i.e., case S2F2, shows that the fatigue might not be an issue for the RC deck when a minimum deck thickness of 7 in is explored as per the MTD 10-20 (Caltrans 2008) because the target service life of 75 years can be reached at a deck thickness of 4.875 in. This tryout case study indicates the high variability of the predicted deck fatigue life while using different model combinations, hence, any potential adoption of these models in bridge deck design requires a sophisticated consideration and highly relies on the experience and judgement of engineers.

These two frameworks are proposed for future studies by the authors of this report based on the current literature review. However, they have not been verified by any laboratory test or on-site investigation. Additionally, the models mentioned in the frameworks are intended for the illustration purpose only and they can be replaced by other alternative models that believed to be more reliable. Since the fatigue issue of either concrete material or RC bridge deck is of interest to many civil engineers, it is possible to conduct more research in the future to examine these two proposed frameworks. Experimental study aiming at measuring the fatigue life of RC bridge decks subjected to realistic moving vehicle loads is always the best approach to deepen the understanding in this research area.

5 APPENDIX

Limited by the scope of the current research, only the force-based framework as introduced in section 4.2 was adopted for the tryout case study to calculate the required thickness of RC bridge deck subjected to cyclic loading. To further ease the calculation process, some assumptions were also made in the following:

(1) Only the standard HL93 truck with 32 kip axle load was considered (P = 16 kip), with an ADTT of 5000 per lane, ignoring the effect of other vehicle types;

(2) The passage of each HL93 truck was equal to 2.5 fatigue cycles;

(3) Load and resistance factors were not considered;

(4) An impact factor of 33% was used per AASHTO;

(5) The tire pressure was assumed to be 133 psi;

(6) A target service life of 75 years, equal to a fatigue life N_f of 342 million cycles, was considered for the RC bridge deck; and

(7) Dry condition was assumed to implement the fatigue model of Matsui (C = 1.52).

This tryout case study aimed to explore the difference in estimated fatigue life of RC bridge decks using different model combinations, hence, the assumptions made above might not be realistic. For example, the HL93 with 32 kip axle is not the only type of truck on the road, the influence of other trucks with different tire patch load also need to be considered for design purpose. In that case, the PM rule as introduced in section 2.3.6 is a promising method to incorporate the effect of other types of vehicles. Of course, a case-by-case investigation is always beneficial to determine the statistical variation on axle loads at the target traffic location.

In the tryout case study, two static models were explored to estimate the local punching shear carrying capacity P_s of the bridge deck, including (a) the fatigue punching shear model of Matsui (1991), referred to as S1; and (b) the general punching shear model (Graddy et al. 2002), referred to as S2. The introduction of these two static models was presented in section 3.3.1. Two fatigue life models were explored to estimate the required thickness of RC bridge deck targeting the service life of 75 years, including (a) the model of Matsui (1991), referred to as F1; (b) the model of El-Ragaby et al. (2007), referred to as F2. The introduction of these two fatigue models was presented to in section 3.3.3. These two static models were explored because of their simplicity for design, also they were both based on the punching shear theory as described in section 3.3.1. Additionally, the using of Matsui's static model was consistent with the fatigue life model as proposed by Matsui. However, the static and fatigue models explored in the combination S2F2 were not derived or calibrated from the same set of test database, and they were proposed by different independent researchers. In other words, the combination S2F2 had never been verified by lab or field test and it was selected only to serve as comparison cases to quantify the difference in predicted fatigue life using different models.

The predicted fatigue life of RC bridge deck is summarized in Table 5-1. The design details of RC bridge deck, e.g., deck thickness, size of reinforcement, spacing of rebars, etc., referred to the MTD 10-20 (Caltrans 2008), and were used as model input to estimate the fatigue life. The bottom and top clear cover was assumed as 1 in and 2 in, respectively. The compressive strength of concrete was assumed as 3250 psi, and the grade 60 rebar with an elastic modulus of 29000 ksi was adopted for this tryout case study. To obtain the target 342 million cycles (75 years), a minimum deck thickness of 7.5 in is required for case S1F1 and 4.875 in for case S2F2. It should be noted that the latter case was calculated based on a tire print size of 12 in × 10 in and did not require the steel reinforcement detail, hence, calculations are not presented for simplicity. However, California requires a minimum deck thickness of 7 in, as a result, the latter case can reach a much longer fatigue life with a 7 in deck thickness and it is far beyond the 342 million cycles threshold, as illustrated in Fig. 5-1. The large variation in the predicted fatigue life is primarily caused by the selection of the static model to estimate the punching shear capacity of the RC deck slab. For example, P_s of case S2 is at least 70% higher than that of case S1, as shown in Table 5-1.

This tryout case study indicates the importance of using an appropriate static model to accurately estimate the punching shear capacity of the RC deck slab. Moreover, a large database from experiments is necessary to examine the reliability of different models as introduced in this review, but the corresponding workload is heavy and beyond the scope of the current research.

Table 5-1 Results of predicted fatigue life using different models

Girder Spacing (ft)	Deck thickness (in)	Rebar size	Rebar spacing (in)	P_s (S1[a]) (kip)	P_s (S2[b]) (kip)	N_f (S1F1[c]) (million cycles)	N_f (S2F2[d]) (million cycles)
4	7	#5	12.00	62.54	114.93	89.93	78780.95
4.25	7	#5	12.00	62.54	114.93	89.93	78780.95
4.5	7	#5	12.00	62.54	114.93	89.93	78780.95
4.75	7	#5	12.00	62.54	114.93	89.93	78780.95
5	7	#5	12.00	62.54	114.93	89.93	78780.95
5.25	7	#5	12.00	62.54	114.93	89.93	78780.95
5.5	7	#5	12.00	62.54	114.93	89.93	78780.95
5.75	7	#5	11.00	64.83	114.93	142.36	78780.95
6	7.125	#5	11.00	65.62	117.79	167.69	99561.84
6.25	7.125	#5	11.00	65.62	117.79	167.69	99561.84
6.5	7.25	#5	11.00	66.41	120.69	197.11	125143.94
6.75	7.375	#5	11.00	67.19	123.61	231.22	156485.21
7	7.5	#5	10.00	70.77	126.56	451.91	194705.88
7.25	7.5	#5	10.00	70.77	126.56	451.91	194705.88
7.5	7.625	#5	10.00	71.58	129.54	528.05	241111.28
7.75	7.75	#5	10.00	72.40	132.55	615.87	297217.32
8	7.75	#5	10.00	72.40	132.55	615.87	297217.32
8.25	7.875	#5	10.00	73.22	135.58	716.98	364778.90
8.5	8	#5	10.00	74.04	138.65	833.20	445821.44
8.75	8.125	#5	10.00	74.86	141.74	966.56	542675.83
9	8.125	#5	10.00	74.86	141.74	966.56	542675.83
9.25	8.25	#5	10.00	75.68	144.86	1119.36	658017.25
9.5	8.375	#5	10.00	76.50	148.01	1294.15	794908.03
9.75	8.375	#5	10.00	76.50	148.01	1294.15	794908.03
10	8.5	#6	12.00	84.87	151.19	4891.14	956845.03
10.25	8.625	#6	11.00	89.12	154.39	9197.06	1147812.00
10.5	8.625	#6	11.00	89.12	154.39	9197.06	1147812.00
10.75	8.75	#6	11.00	90.06	157.63	10590.65	1372337.27
11	8.875	#6	11.00	91.00	160.89	12176.61	1635557.37
11.25	8.875	#6	11.00	91.00	160.89	12176.61	1635557.37
11.5	9	#6	11.00	91.94	164.19	13978.95	1943287.04
11.75	9.125	#6	11.00	92.88	167.51	16024.39	2302096.29
12	9.125	#6	10.00	96.93	167.51	27634.21	2302096.29
12.25	9.25	#6	10.00	97.91	170.86	31631.96	2719395.21

12.5	9.375	#6	10.00	98.89	174.23	36156.84	3203527.14
12.75	9.5	#6	10.00	99.87	177.64	41271.75	3763871.05
13	9.5	#6	10.00	99.87	177.64	41271.75	3763871.05
13.25	9.625	#6	10.00	100.85	181.07	47046.33	4410954.10
13.5	9.75	#6	10.00	101.83	184.54	53557.58	5156575.20
13.75	9.75	#6	10.00	101.83	184.54	53557.58	5156575.20
14	9.875	#6	10.00	102.81	188.03	60890.59	6013940.75
14.25	10	#6	10.00	103.79	191.55	69139.26	6997813.70
14.5	10.125	#6	10.00	104.77	194.49	78407.11	7921749.54
14.75	10.25	#6	10.00	105.75	197.45	88808.19	8951646.89
15	10.375	#6	10.00	106.73	200.41	100467.98	10097949.76

Note: [a]punching shear model proposed by Matsui (1991); [b]general punching shear model (Graddy et al. 2002); [c]static and fatigue model of Matsui (1991); and [d]general punching shear model (Graddy et al. 2002) and fatigue model of El-Ragaby et al. (2007). Combination S2F2 had never been verified by lab or field test and it was selected only to serve as a comparison case to quantify the difference in predicted fatigue life using different models.

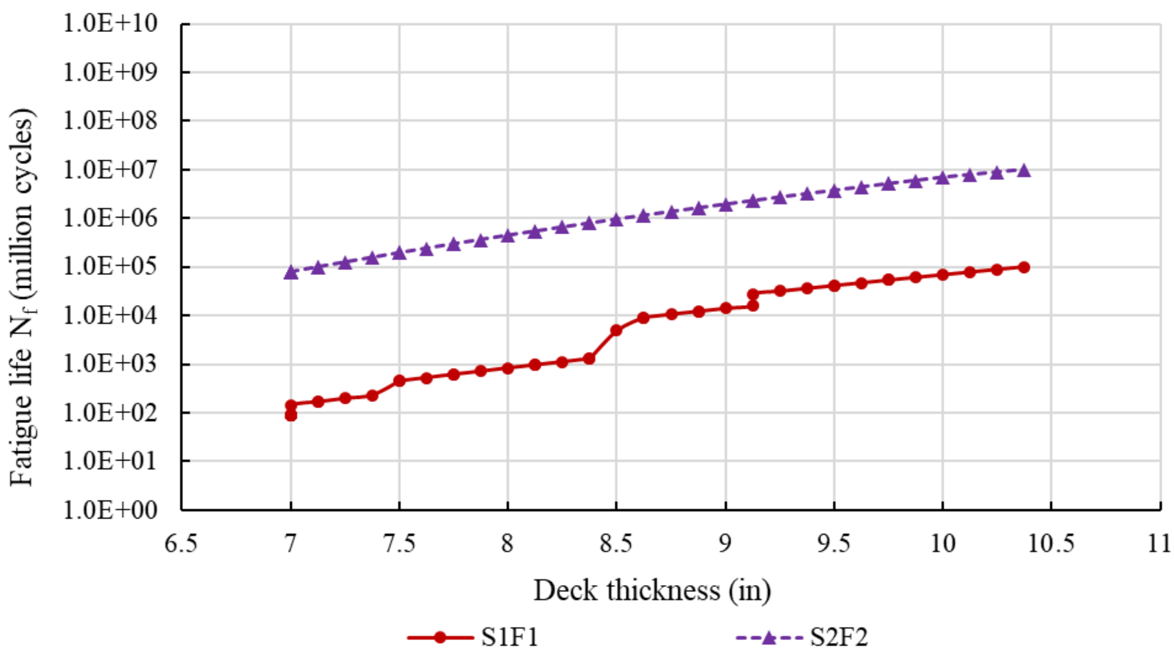

Fig. 5-1 Comparison of predicted fatigue life using different models

REFERENCES

Aas-Jakobsen, K. (1970). Fatigue of concrete beams and columns. Division of Concrete Structures, Norwegian Inst. of Technology, University of Trondheim.

ACI 215R-74 (Revised 1992/Reapproved 1997). Considerations for Design of Concrete Structures Subjected to Fatigue Loading. ACI Committee 215.

ACI Committee. (2019). Building code requirements for structural concrete (ACI 318-19) and commentary. American Concrete Institute.

American Association of State Highway and Transportation Officials. (2017). AASHTO LRFD bridge design specifications, customary U.S. units. Washington, DC: American Association of State Highway and Transportation Officials.

Bakht, B., & Lam, C. (2000). Behavior of transverse confining systems for steel-free deck slabs. *Journal of Bridge Engineering*, 5(2), 139-147.

Bode, M., & Marx, S. (2021). Energetic damage analysis regarding the fatigue of concrete. *Structural Concrete*, 22, E851-E859.

Buyukozturk, O., & Tseng, T. M. (1984). Concrete in biaxial cyclic compression. *Journal of Structural Engineering*, 110(3), 461-476.

Caltrans (2008). Memo to Designers 10-20 Attachment 2. Available at: <https://dot.ca.gov/programs/engineering-services/manuals/memo-to-designers>

Cornelissen, H. A. W., & Reinhardt, H. W. (1984). Uniaxial tensile fatigue failure of concrete under constant-amplitude and programme loading. *Magazine of Concrete Research*, 36(129), 216-226.

Csagoly, P. F., & Lybas, J. M. (1989). Advanced design method for concrete bridge deck slabs. *Concrete International*, 11(5), 53-63.

Cuelho, E., & Stephens, J. (2013). Investigation of Methacrylate Rehabilitation Strategy to Extend the Service Life of Concrete Bridge Decks (No. CA13-1723).

Drar, A. A. M., & Matsumoto, T. (2016). Fatigue analysis of RC deck slabs reinforced with plain bars based on the bridging stress degradation concept. *Journal of Advanced Concrete Technology*, 14(1), 21-34.

El-Ragaby, A., El-Salakawy, E., & Benmokrane, B. (2007). Fatigue life evaluation of concrete bridge deck slabs reinforced with glass FRP composite bars. *Journal of Composites for Construction*, 11(3), 258-268.

Fang, I. K., Tsui, C. K. T., Burns, N. H., & Klingner, R. E. (1990). Load capacity of isotropically reinforced, cast-in-place and precast panel bridge decks. *PCI Journal*, 35(4), 104-107.

FIB (2013). Fib model code for concrete structures 2010.

Gao, L., & Hsu, C. T. T. (1998). Fatigue of concrete under uniaxial compression cyclic loading. Materials Journal, 95(5), 575-581.

Graddy, J. C., Kim, J., Whitt, J. H., Burns, N. H., & Klingner, R. E. (2002). Punching-shear behavior of bridge decks under fatigue loading. *Structural Journal*, 99(3), 257-266.

Hewitt, B. E., & Batchelor, B. D. (1975). Punching shear strength of restrained slabs. *Journal of the Structural Division*, 101(9), 1837-1853.

Hilsdorf, H. K., & Kesler, C. E. (1966, October). Fatigue strength of concrete under varying flexural stresses. In *Journal Proceedings* (Vol. 63, No. 10, pp. 1059-1076).

Holmen, J. O. (1982). Fatigue of concrete by constant and variable amplitude loading. *Special Publication*, 75, 71-110.

Hsu, T. T. (1981, July). Fatigue of plain concrete. In *Journal Proceedings* (Vol. 78, No. 4, pp. 292-305).

Isojeh, B., El-Zeghayar, M., & Vecchio, F. J. (2017). Concrete damage under fatigue loading in uniaxial compression. *ACI Materials Journal*, 114(2), 225-235.

Kennedy, G., & Goodchild, C. (2004). Practical yield line design. Concrete Centre, Surrey, UK.

Kinnunen, S., & Nylander, H. (1960). Punching of concrete slabs without shear reinforcement (p. 112). New York: Elander.

Kolluru, S. V., O'Neil, E. F., Popovics, J. S., & Shah, S. P. (2000). Crack propagation in flexural fatigue of concrete. *Journal of Engineering Mechanics*, 126(9), 891-898.

Lei, D., Zhang, P., He, J., Bai, P., & Zhu, F. (2017). Fatigue life prediction method of concrete based on energy dissipation. *Construction and Building Materials*, 145, 419-425.

Lohaus, L., Oneschkow, N., & Wefer, M. (2012). Design model for the fatigue behaviour of normal-strength, high-strength and ultra-high-strength concrete. *Structural Concrete*, 13(3), 182-192.

Maeda, Y., & Matsui, S. (1984). Fatigue of reinforced concrete slabs under trucking wheel load. *Proceedings of JCI*, 6, 221-224.

Maekawa, K., & El-Kashif, K. F. (2004). Cyclic cumulative damaging of reinforced concrete in post-peak regions. *Journal of Advanced Concrete Technology*, 2(2), 257-271.

Maekawa, K., Gebreyouhannes, E., Mishima, T., & An, X. (2006a). Three-dimensional fatigue simulation of RC deck slabs under traveling wheel-type loads. *Journal of Advanced Concrete Technology*, 4(3), 445-457.

Maekawa, K., Okamura, H., & Pimanmas, A. (2003). Non-linear mechanics of reinforced concrete. CRC Press.

Maekawa, K., Toongoenthong, K., Gebreyouhannes, E., & Kishi, T. (2006b). Direct path-integral scheme for fatigue simulation of reinforced concrete in shear. *Journal of Advanced Concrete Technology*, 4(1), 159-177.

Matsui, S. (1991). Prediction of fatigue life of reinforced concrete slabs of highway bridges. *Japan Society for Safety Engineering*, 30(6), 432-440 (in Japanese).

McCall, J. T. (1958, August). Probability of fatigue failure of plain concrete. In *Journal Proceedings* (Vol. 55, No. 8, pp. 233-244).

Miner, M.A. (1945). Cumulative Damage in Fatigue. *Journal of Applied Mechanics*, 3, 159-164.

Mufti, A. A., & Newhook, J. P. (1998). Punching shear strength of restrained concrete bridge deck slabs. *Structural Journal*, 95(4), 375-381.

Okada, K., Okamura, H., & Sonoda, K. (1978). Fatigue failure mechanism of reinforced concrete bridge deck slabs. *Transportation Research Record*, 664, 136-144.

Ortega, J. J., Ruiz, G., Rena, C. Y., Afanador-Garcia, N., Tarifa, M., Poveda, E., ... & Evangelista Jr, F. (2018). Number of tests and corresponding error in concrete fatigue. *International Journal of Fatigue*, 116, 210-219.

Palmgren, A.G. (1924). Die Lebensdauer von Kugellagern (Life Length of Roller Bearings or Durability of Ball Bearings). *Zeitschrift des Vereines Deutscher Ingenieure (ZVDI)*, 14, 339-341.

Perdikaris, P. C., & Beim, S. (1988). RC bridge decks under pulsating and moving load. *Journal of Structural Engineering*, 114(3), 591-607.

Petkovic, G., Lenschow, R., Stemland, H., & Rosseland, S. (1990). Fatigue of high-strength concrete. *Special Publication*, 121, 505-526.

Petryna, Y. S., Pfanner, D., Stangenberg, F., & Krätzig, W. B. (2002). Reliability of reinforced concrete structures under fatigue. *Reliability Engineering & System Safety*, 77(3), 253-261.

Reinhardt, H. W., & Cornelissen, H. A. W. (1984). Post-peak cyclic behaviour of concrete in uniaxial tensile and alternating tensile and compressive loading. *Cement and Concrete Research*, 14(2), 263-270.

Rüsch, H. (1960). Researches toward a general flexural theory for structural concrete. *Journal of the American Concrete Institute*, 57(1), 1-28.

Saucedo, L., Rena, C. Y., Medeiros, A., Zhang, X., & Ruiz, G. (2013). A probabilistic fatigue model based on the initial distribution to consider frequency effect in plain and fiber reinforced concrete. *International Journal of Fatigue*, 48, 308-318.

Schläfli, M., & Brühwiler, E. (1998). Fatigue of existing reinforced concrete bridge deck slabs. *Engineering Structures*, 20(11), 991-998.

Shakushiro, K., Mitamura, H., Watanabe, T., & Kishi, N. (2011). Experimental study on fatigue durability of RC deck slabs reinforced with round steel bars. *Journal of Structural Engineering*, 57, 1297-1304.

Song, Z., Frühwirt, T., & Konietzky, H. (2018). Characteristics of dissipated energy of concrete subjected to cyclic loading. *Construction and Building Materials*, 168, 47-60.

Sonoda, K., & Horikawa, T. (1982). Fatigue strength of reinforced concrete slabs under moving loads. *Fatigue of Steel and Concrete Structures*, 455-462.

Sparks, Peter R., and J. B. Menzies. "The effect of rate of loading upon the static and fatigue strengths of plain concrete in compression." Magazine of Concrete Research 25.83 (1973): 73-80.

Su, E. C., & Hsu, T. T. (1988). Biaxial Compression Fatigue and the Discontinuity of Concrete. *Materials Journal*, 85(3), 178-188.

Subramaniam, K. V., Popovics, J. S., & Shah, S. P. (2002). Fatigue fracture of concrete subjected to biaxial stresses in the tensile C-T Region. *Journal of Engineering Mechanics*, 128(6), 668-676.

Sun, W., Mu, R., Luo, X., & Miao, C. (2002). Effect of chloride salt, freeze–thaw cycling and externally applied load on the performance of the concrete. *Cement and Concrete Research*, 32(12), 1859-1864.

Suthiwarapirak, P., & Matsumoto, T. (2006). Fatigue analysis of RC deck slabs and repaired RC deck slabs based on crack bridging degradation concept. *Journal of Structural Engineering*, 132(6), 939-948.

Taliercio, A. L. F., & Gobbi, E. (1996). Experimental investigation on the triaxial fatigue behaviour of plain concrete. *Magazine of Concrete Research*, 48(176), 157-172.

Tauskela, L. M. (2020). Testing A Full-Scale Reinforced Concrete Bridge Deck with GFRP and Steel Reinforcement Using Cyclic Pulsating and Rolling Loads. Master's Thesis, Queen's University, 2020

Tepfers, R. (1982). Fatigue of plain concrete subjected to stress reversals. *Special Publication*, 75, 195-216.

Tepfers, R., & Kutti, T. (1979, May). Fatigue strength of plain, ordinary, and lightweight concrete. In *Journal Proceedings* (Vol. 76, No. 5, pp. 635-652).

Tepfers, R., Görlin, J., & Samuelsson, T. (1973). Concrete subjected to pulsating load and pulsating deformation of different pulse waveform. *Nordisk betong*, 17(4).

Tepfers, R., Hedberg, B., & Szczekocki, G. (1984). Absorption of energy in fatigue loading of plain concrete. *Matériaux et Construction*, 17(1), 59-64.

Torrenti, J. M., Pijaudier-Cabot, G., & Reynouard, J. M. (Eds.). (2013). Mechanical behavior of concrete. John Wiley & Sons.

Yoshitake, I., Kim, Y. J., Yumikura, K., & Hamada, S. (2010). Moving-wheel fatigue for bridge decks strengthened with CFRP strips subject to negative bending. *Journal of Composites for Construction*, 14(6), 784-790.

Youn, S. G., & Chang, S. P. (1998). Behavior of composite bridge decks subjected to static and fatigue loading. *Structural Journal*, 95(3), 249-258.

Zhang, B., Phillips, D. V., & Green, D. R. (1998). Sustained loading effect on the fatigue life of plain concrete. *Magazine of Concrete Research*, 50(3), 263-278.

Zhang, B., Phillips, D. V., & Wu, K. (1996). Effects of loading frequency and stress reversal on fatigue life of plain concrete. *Magazine of Concrete Research*, 48(177), 361-375.